Uveitis and Intraocular Inflammation

10

Nazanin Ebrahimiadib, Kaveh Fadakar, Samaneh Davoudi, Charles Stephen Foster, and Fedra Hajizadeh

Abstract

This chapter contains an interesting collection of OCT images of a variety of uveitis diseases and the characteristic features of each have been explained. This starts with uveitis cystoid macular edema and continues with Behçet's disease, toxoplasma retinochoroiditis, serpiginous choroiditis, other white dot syndromes (multiple evanescent white dot syndrome, acute zonal occult outer retinopathy, acute posterior multifocal placoid pigment epitheliopathy and multifocal choroiditis with panuveitis), and tuberculous choroiditis. In addition, unique feature of inflammatory choroidal neovascularization has been explained. It contains diagnostic tips of not only OCT but other imaging modalities such as enhanced-depth imaging, fluorescein angiography, indocyanine green angiography, echography, and the visual field. It highlights common and differentiating hallmarks of posterior scleritis and Vogt–Koyanagi–Harada disease and features to consider a patient in remission. Another valuable aspect of this chapter is that follow-up images are included to highlight changes with time or treatment. Rare diseases such as idiopathic retinal vasculitis, aneurysm, and neuroretinitis (IRVAN) and vascular accident in the setting of viral retinitis have also been demonstrated.

N. Ebrahimiadib (✉) · K. Fadakar
Eye Research Center, Farabi Eye Hospital, Tehran University of Medical Sciences, Tehran, Iran
e-mail: nebrahimiadib@ufl.edu

S. Davoudi
Department of Ophthalmology, University of Florida, Gainesville, FL, USA

C. S. Foster (✉)
Massachusetts Eye Research and Surgery Institution (MERSI) Ocular Immunology &Uveitis Foundation, 1440 Main St. Suite 201, Waltham, MA 02451, USA
e-mail: fosters@uveitis.org

F. Hajizadeh
Noor Ophthalmology Research Center, Noor Eye Hospital, No. 96, Esfandiar Blvd., Vali'asr Ave., Tehran, Iran
e-mail: fhajizadeh@noorvision.com

10.1 General Effects of Intraocular Inflammation in the Posterior Pole

The major cause of reduced vision in patients with uveitis is macular edema, which affects 30–44% of patients with uveitis [1] (Figs. 10.1 and 10.2). It is often associated with pars planitis, iridocyclitis, and posterior uveitis. Three patterns have been described in uveitic macular edema: focal, diffuse, and cystoid (Fig. 10.2) [2]. Uveitic macular edema usually involves the center 1 mm and the inner 3 mm of ETDRS grid. Additionally, it first emerges as small parafoveal INL cysts, followed by larger OPL/ONL cysts and finally SRF develops in 65% of the eyes [3]. To detect diffuse macular edema where cystic spaces are absent, OCT thickness is helpful which shows thickening as hot areas especially in perifoveal retina (Fig. 10.1). It has been shown that perifoveal thickening is associated with uveitis activity in eyes with intermediate or panuveitis [3].
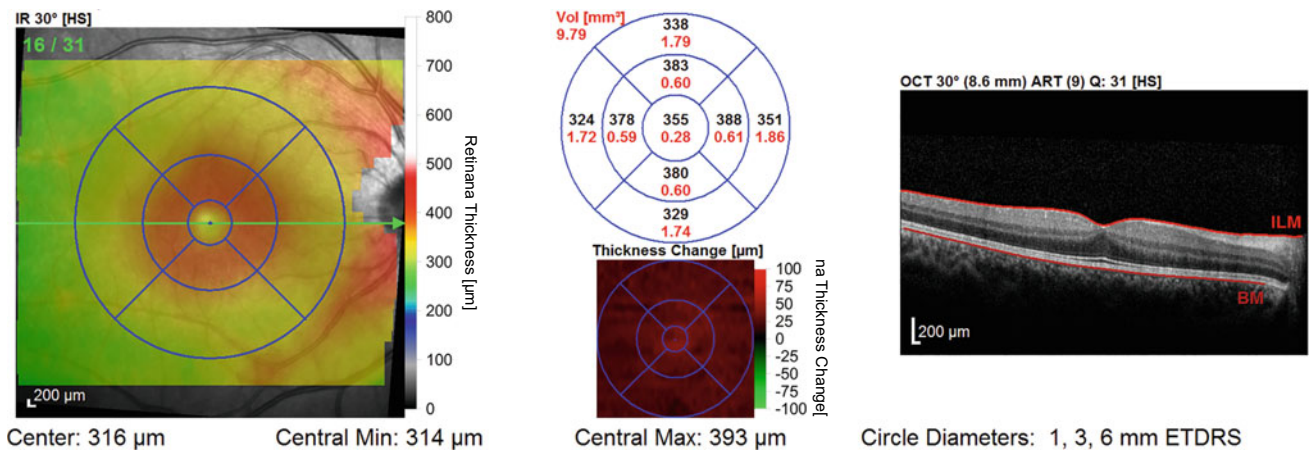
Fig. 10.1 The topographic map and OCT of a patient with active uveitis. Although the central foveal pit is preserved, there is a spongy edema especially in the perifoveal area which is best evident in topographic map
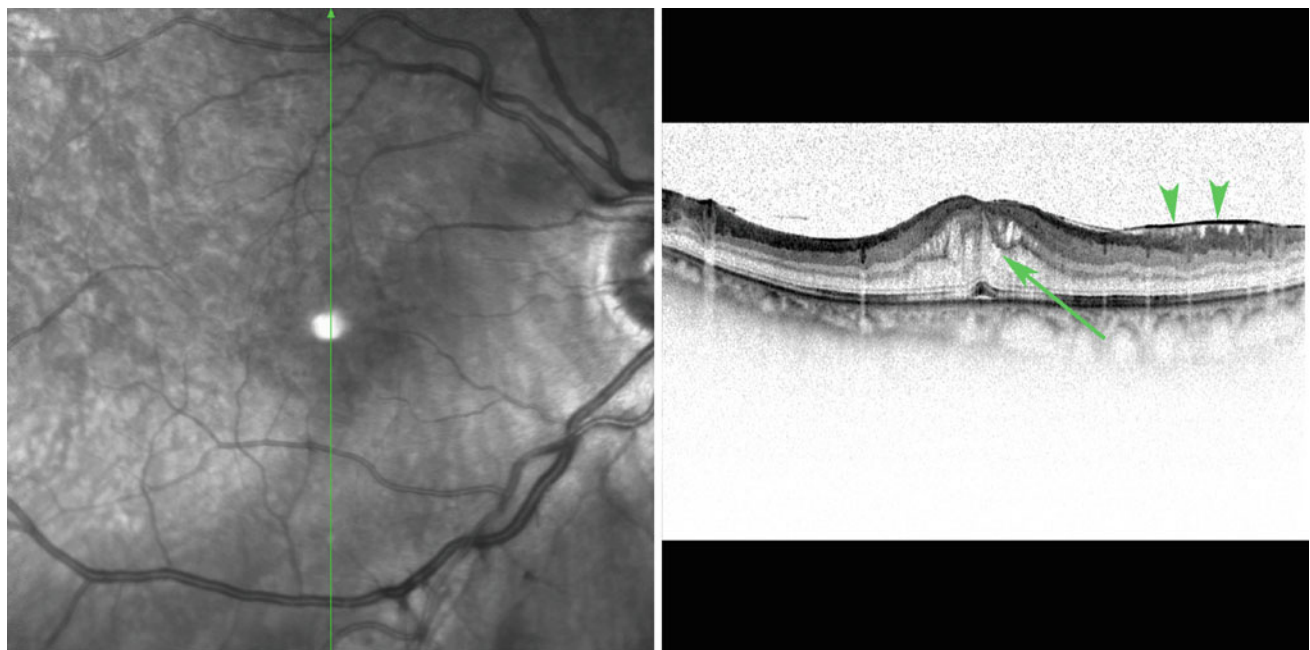

Fig. 10.2 Cystoid foveal edema (*green arrow*) accompanied by small subfoveal retinal detachment is a hallmark sign in intraocular inflammation. Generalized macular thickening can also occur. Epiretinal membrane formation (*green arrowheads*) is a frequent finding in cases of recurrent intraocular inflammation

Infiltration of inflammatory cells and protein-rich exudates into vitreous cavity results in hazy media which is clinically discerned as vitritis. Resolution of current OCT devices is not sufficient to detect cell particles in vitreous space; however, clumps of these cells can be detected as floating punctate spots [4]. These spots indicate active uveitis; however, they do not fade immediately after that the acute episode of acute inflammation has subsided [5].

Inflammatory CNV (iCNV) may arise secondary to some uveitic entities which primarily involve the choroid such as multifocal choroiditis and serpiginous choroiditis. These lesions usually develop between neurosensory retina and RPE, characterized as type II CNV [6]. OCT features suggestive for iCNV include an increase in subretinal, hyper-reflective material and adjacent subretinal fluid. Occasionally, an undulating flat PED with mixed reflectivity can be appreciated as an occult type I CNV, along with the main type II lesion [7]. The so called "pitchfork sign" is a distinct feature that was first described in iCNV. It is characterized by finger-like hyper-reflective projections extending from CNV membrane through outer retina [8]. Differentiation of an iCNV from an inflammatory choroidal granuloma and even a subretinal fibrosis is sometimes challenging. OCTA can be of help in this instances by showing a vascular tuft which confirms an iCNV.

Inflammatory macular holes can develop in intraocular inflammations with the history of long-standing macular edema. Nonsurgical management such as immunosuppressive therapy or local injection of corticosteroids should be considered as the first treatment approach, however long-standing cases may require surgery. Reopening of these holes, especially during reactivation of uveitis may occur that may require vitrectomy [9].

10.2 Behcet's Disease

Behcet's disease is a chronic autoimmune disorder affecting vessels of multiple organs in the body. Retinal vasculitis is a vision threatening complication of the disease that has characteristic features in fluorescein angiography and OCT. (Figs. 10.3 and 10.4).

Among diagnostic features of Behcet's disease are transient retinal infiltrates which may appear during exacerbation [10]. OCT section through the lesion demonstrates, focal retinal thickening, blurred increased hyper-reflectivity of inner retina with corresponding optical shadowing. These lesions rapidly resolve without evident clinical scar; however, OCT illustrates an inner retinal atrophy in its wake.

Subfoveal choroidal depth is mildly increased in the acute phase of inflammation in Behcet's uveitis, compared to the remission phase [11, 12]. In a study from Turkey, subfoveal choroidal thinning was observed in the later stages of the disease, which may be related to progressive choroidal fibrosis and thinning due to ischemic changes from chronic inflammation [13].

10.3 Vogt–Koyanagi–Harada Disease

Vogt–Koyanagi–Harada is a multisystemic disorder which can affect uveal tract, central nervous system, hair and skin. In eye, it usually manifests as a bilateral granulomatous panuveitis with multiple exudative retinal detachment. Fluorescein angiography in acute phase is of diagnostic value (Fig. 10.5).

Optical coherence tomography (OCT) has characteristic features in this disease. In the acute phase of Vogt–Koyanagi–Harada (VKH) high retinal detachment (>400 microns) and subretinal cystoid spaces form with septate membrane in these spaces [14].

Hyperreflective subretinal dots that have been described in VKH may represent inflammatory cells and shed photoreceptor outer segments engulfed by macrophages, similar to the description of dots in central serous chorioretinopathy (CSCR) described by Spaide [15] and other authors [16]. Yamamoto et al. [17] demonstrated a significant increase in inner retinal thickness (i.e., from the internal limiting membrane [ILM] to the inner plexiform layer) in the acute period of VKH, compared to the convalescent phase (Figs. 10.6, 10.7, 10.8 and 10.9).

Intraretinal septates can be seen in OCT in acute phase. A separation occurs at the level of photoreceptors, between outer segment and inner segment myoid, which is called "bacillary layer detachment" (Fig. 10.7). This phenomenon
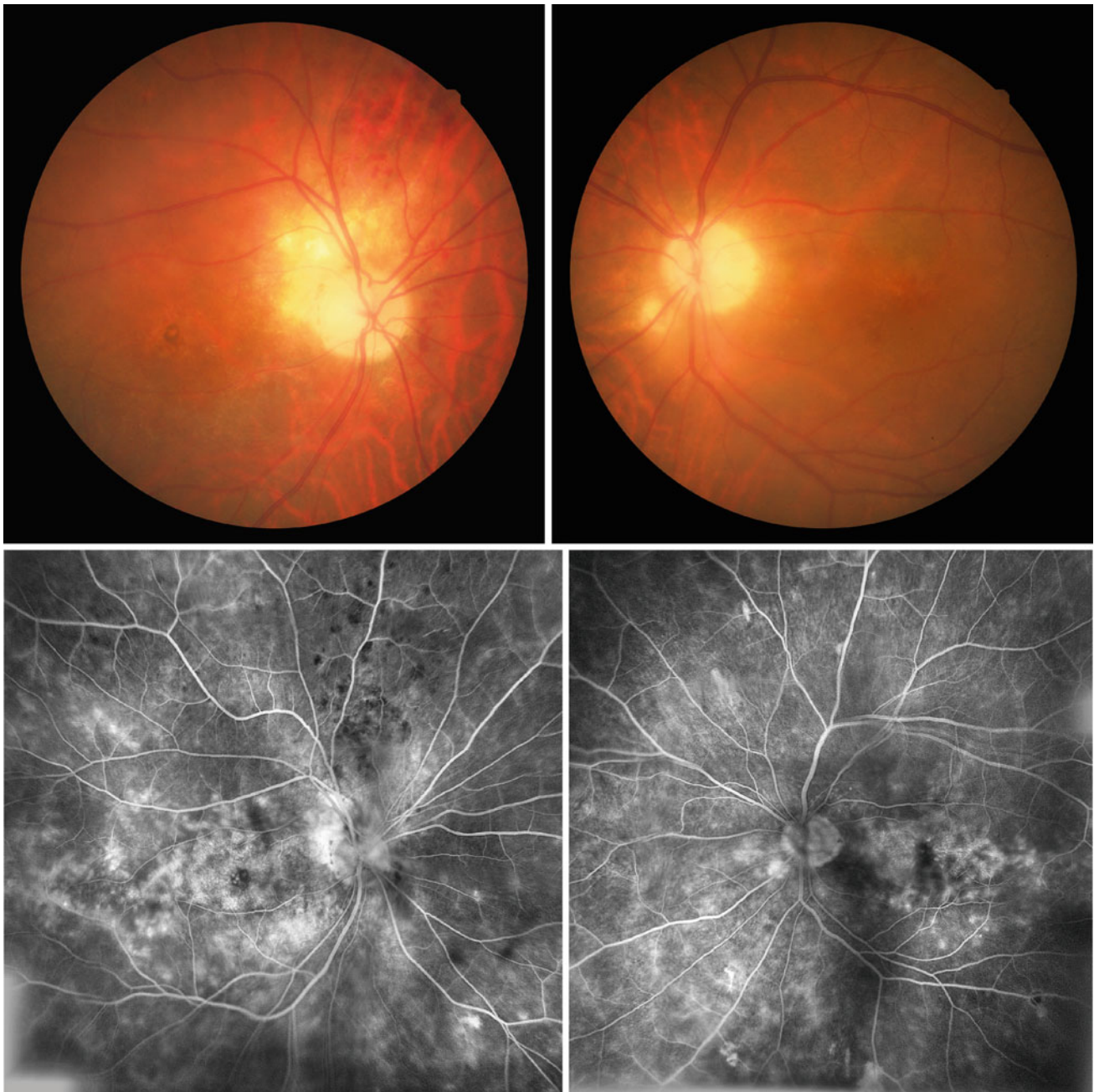
Fig. 10.3 Color fundus photographs and fluorescein angiography images of the retina of a 43 year-old man with a 12 year history of poorly managed Bechet's disease. Visual acuity in the right and left eye is less than 20/200 and 20/160, respectively. Bilateral optic atrophy in the fundus photographs (*upper images*), and widespread capillary occlusion, staining, and vascular leakage in the late phase angiography images (*lower images*) are remarkable

is not characteristics for VKH and has been described in other inflammatory or non-inflammatory ocular conditions.

Choroidal thickness increases during the acute stage of VKH and returns to normal after treatment. Enhanced depth imaging optical coherence tomography (EDI-OCT) can detect this change and is a helpful technique in monitoring disease activity. With the recurrence of disease, rebound thickening of the choroid occurs [18].

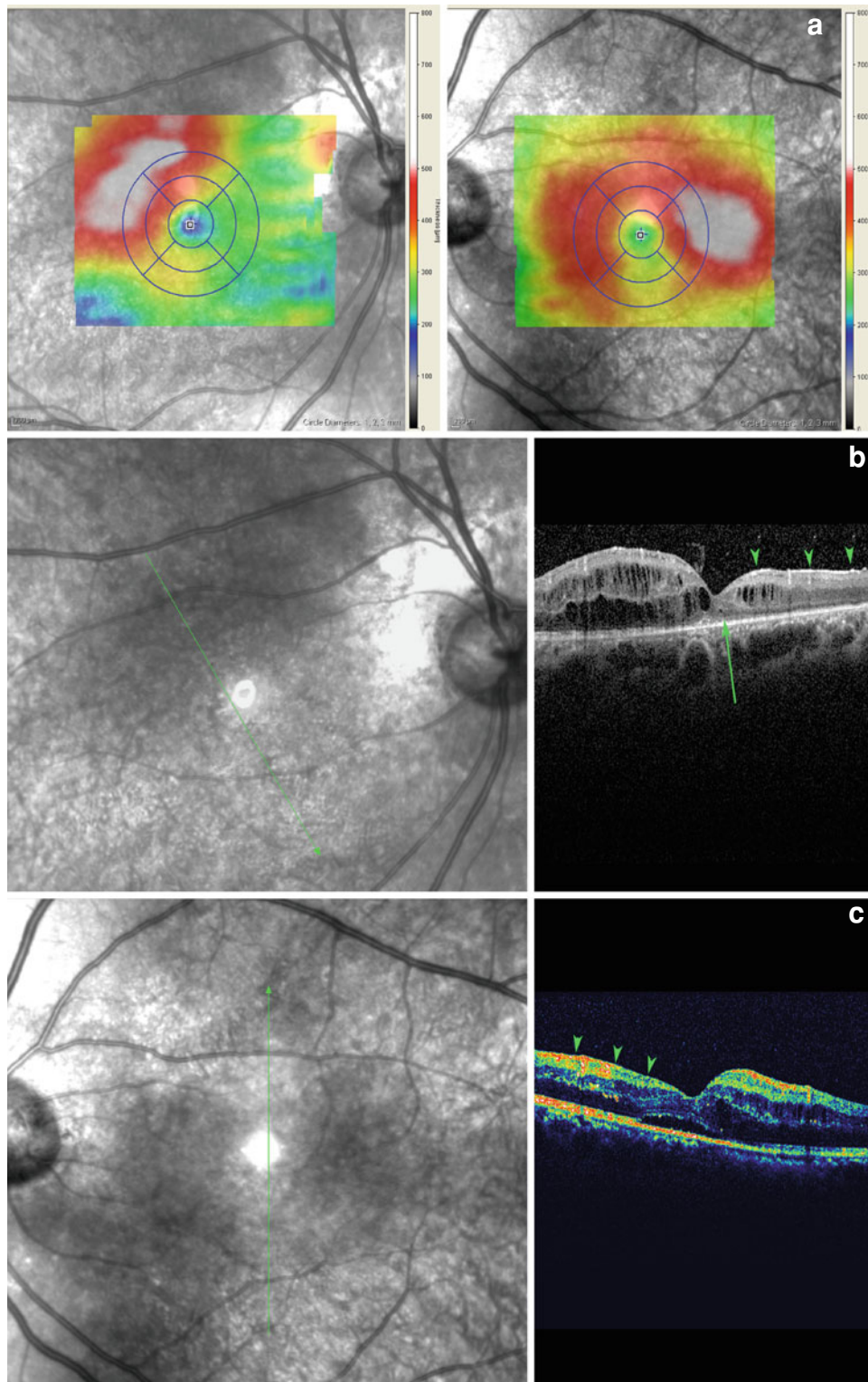Enhanced depth imaging optical coherence tomography has also demonstrated that choroid thickness reduces during

Fig. 10.4 a The topographic maps of the patient in Fig. 10.3 show edematous and atrophic areas in the macula. **b** The SLO-OCT image of the right eye shows cystic macular edema with tissue loss that is compatible with longstanding edema and foveal ellipsoid zone disruption with outer nuclear layer atrophy (*green arrow*). These findings predict poor visual outcome, even after the resolution of edema. Retinal nerve fiber layer atrophy (*green arrowheads*) occurs because of inflammatory or ischemic injury to the ganglion cell axons (e.g., small macular BRVOs or capillary nonperfusion). This pattern usually occurs in vasculitis. **c** The SLO-OCT image of the left eye illustrates diffuse cystoid macular edema and a small subfoveal serous detachment. The ellipsoid zone is partially preserved with better vision in this eye. Atrophy of the inner layers (*green arrowheads*) in the inferior part of macula is associated with occlusive vasculitis, microvasculopathy, capillary nonperfusion, and small BRVOs. *BRVO* branch retinal vein occlusion
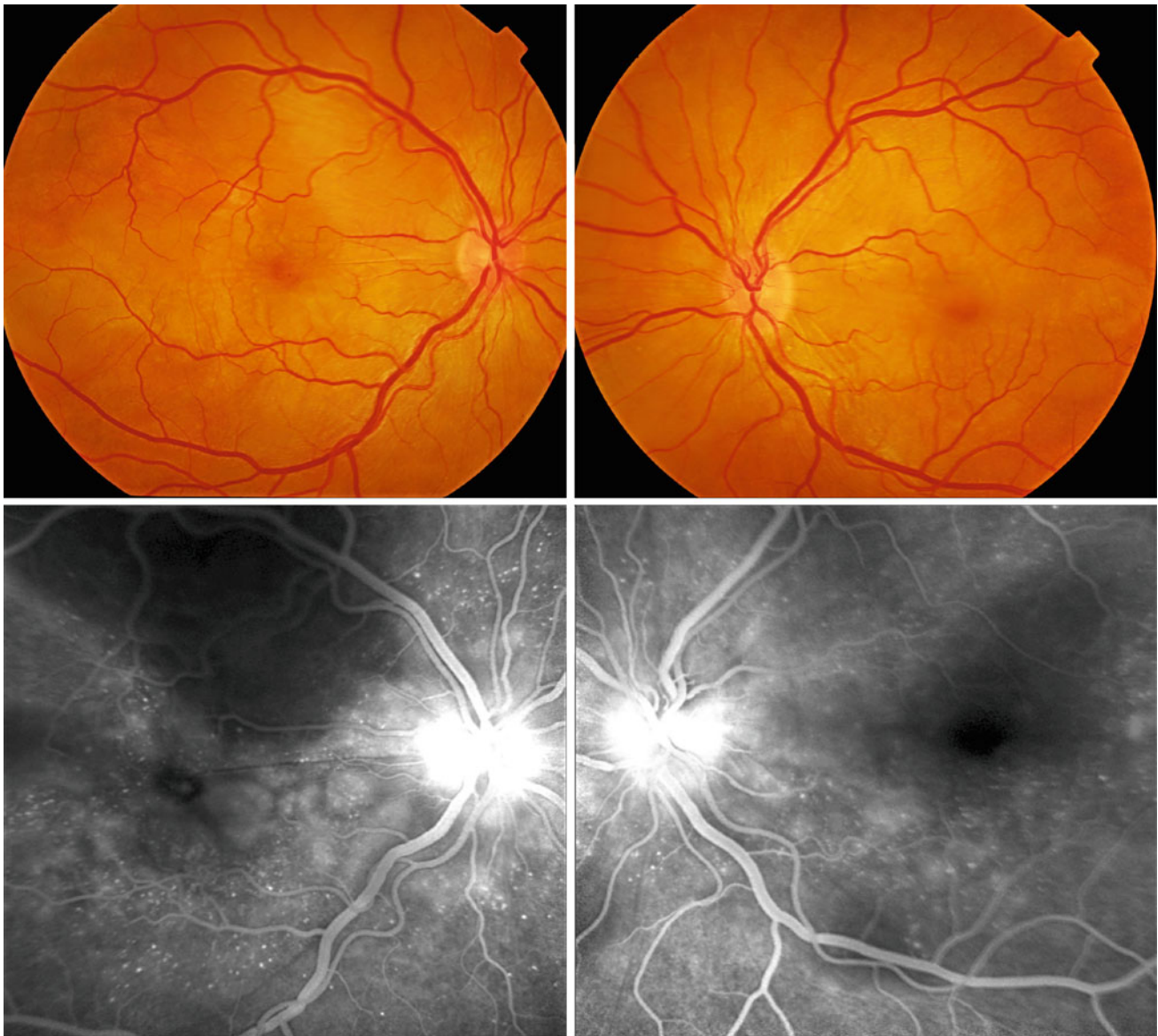
Fig. 10.5 The color fundus photographs and fluorescein angiography (FA) images are from a patient in the acute phase of VKH disease. In the color fundus photograph, multiple pale serous detachments that extend centrifugally from the optic disc in both eyes are the hallmark sign of VKH disease. In the FA image, serous detachment of the retina appears as hypofluorescent areas. In addition, multiple pinpoint hyperfluorescent dots and disc hyperfluorescence in the late stage of fluorescein angiography are characteristic angiographic findings in VKH disease. *VKH* Vogt–Koyanagi–Harada

the chronic phase. Subchoroidal thickness is inversely correlated with the amount of fundus pigmentation, the area of peripapillary atrophy, and the duration of the disease [19].

Choroidal folds are another finding that can be observed in 52–71% of cases of VKH in the acute phase. These choroidal folds are wrinkles in the RPE, Bruch's membrane, and inner choroid that radiate from the optic disc to the periphery. Inflammation and thickening of the choroid mechanically compress the RPE and Bruch's membrane and optic nerve, which contributes to inward bulging of the choroid and optic disc swelling. The sclera is less flexible than the retina; therefore, choroidal infiltration and exudation cause bumpy deformation toward the retina and the formation of choroidal folds [20]. Wrinkling of the ILM is another finding in the acute stage [14]. The presence of a choroidal fold may indicate a more chronic and severe disease and
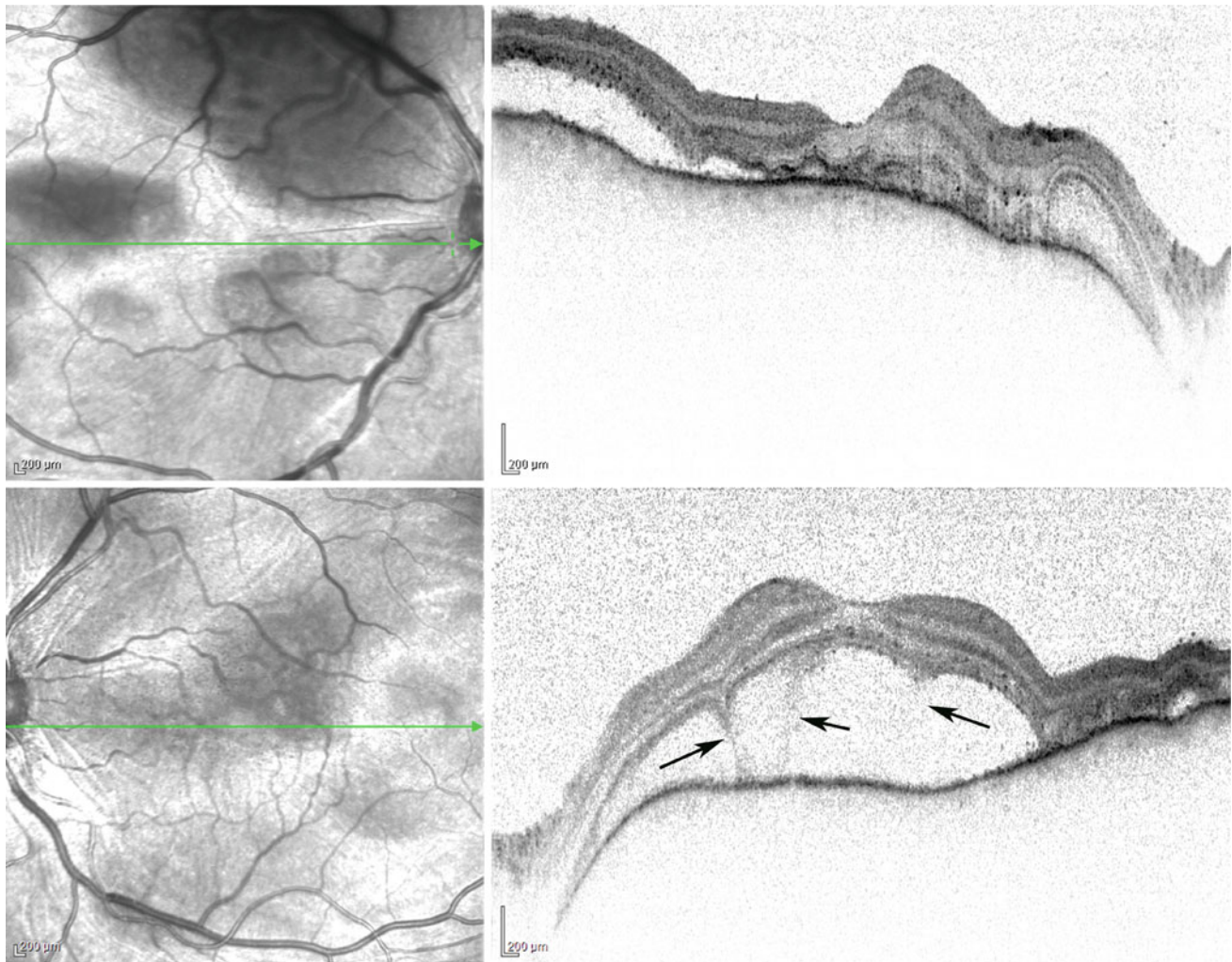
Fig. 10.6 The two SLO-OCT cuts of both eyes of the patient in Fig. 10.5 crossed through the central fovea and illustrate the typical OCT signs of VKH disease. Multiple serofibrinous detachments with numerous small dots at the outer border of the detached retina, thickening of outer border of photoreceptors, and disorganization of the outer retina are OCT findings in patients with VKH disease. The detached retina is often connected to the RPE layer by multiple bridges (*arrows*). *RPE* retinal pigment epithelium, *SLO-OCT* scanning laser ophthalmoscopy optical coherence tomography, *VKH* Vogt–Koyanagi–Harada

therefore requires meticulous follow up and aggressive treatment to prevent a sunset glow fundus [21]. This feature is very helpful because it is difficult to differentiate between active ongoing inflammations with an old choroidal stromal scar by using indocyanine green (ICG) angiography. In ICG angiography, both appear as hypofluorescent dark dots. In rare cases of recurrence of the disease, there may be no subretinal fluid or visual acuity deterioration. However, observing RPE folds on OCT necessitates prompt treatment [22].

Acute or chronic phase VKH causes loss of the vascular pattern of the inner choroid and increase in homogeneity of the choroid which can be detected on EDI-OCT, This finding is secondary to inflammatory granulomas in the choroid [23] (Figs. 10.10, 10.11, 10.12 and 10.13).
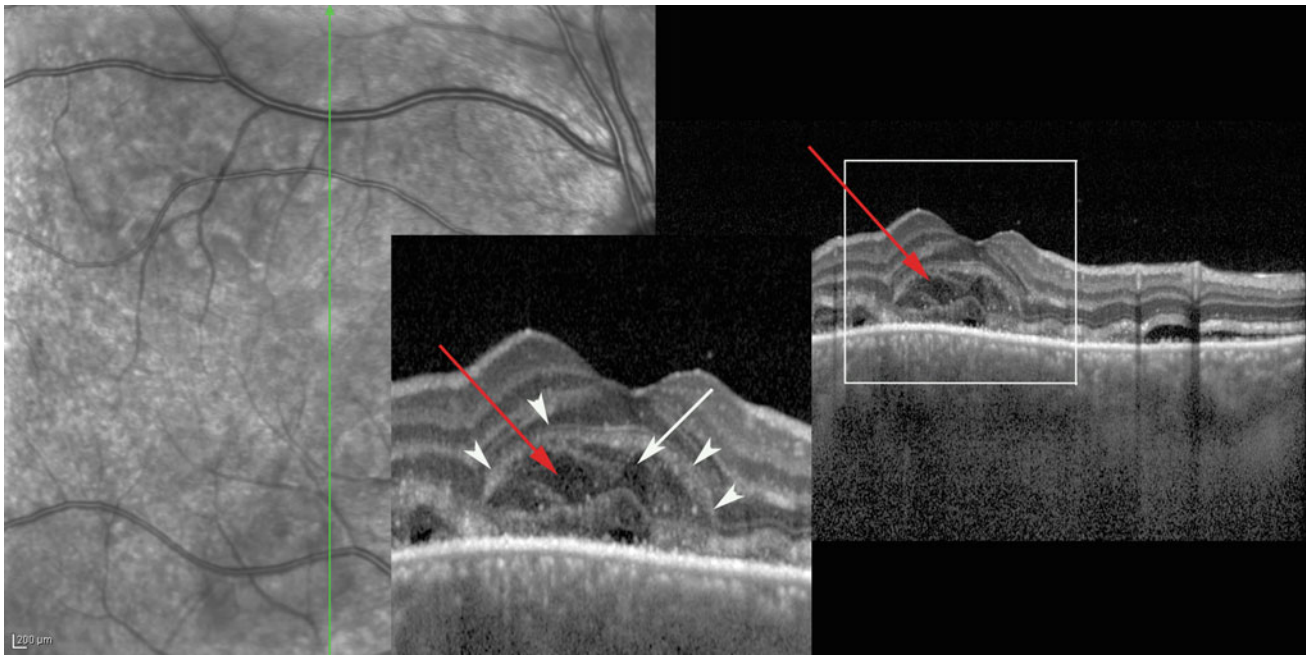
Fig. 10.7 The SLO-OCT images are from a patient with acute stage VKH. Intraretinal cystoid spaces (*white arrows*) with thickening of external limiting membrane (*white arrowheads*) are characteristics of VKH disease. "Bacillary layer detachment" is shown by red arrows. *SLO-OCT* scanning laser ophthalmoscopy optical coherence tomography, *VKH* Vogt–Koyanagi–Harada

Sunset glow fundus: The sunset glow fundus is the convalescent phase of the VKH disease, and develops 12 weeks after disease onset. In this phase, the choroid is atrophic with dropout choriocapillaris [24] (Fig. 10.14).

10.4 Posterior Scleritis

Posterior scleritis has similar findings with VKH disease (Figs. 10.15, 10.16, 10.17, 10.18 and 10.19).

The choroid is in close apposition to the sclera; therefore, it may be affected during acute episodes of posterior scleritis. Thickening of the subfoveal choroid in acute attacks of posterior scleritis and its thinning with recurrent episodes has been demonstrated [25, 26].

10.5 Toxoplasma Retinochoroiditis

The active lesion in ocular toxoplasmosis is choroiditis and retinitis with a blurred reflective appearance in the inner retinal layers and a full-thickness retinal disorganization on OCT. Orefice et al. [27] called this finding as the "smudge effect." The lesion occupies the full thickness of the retina, which causes disorganization and the total loss of lamination of the retinal layers. It is hyperreflective with the most hyperreflectivity in the inner retinal layers. Posterior shadowing is also present; however, with the aid of EDI-OCT, a choroidal hyporeflective area compatible with toxoplasma choroidal granuloma is sometimes discernible. (Fig. 10.20) Some changes in the retinal pigment epithelium (RPE)/
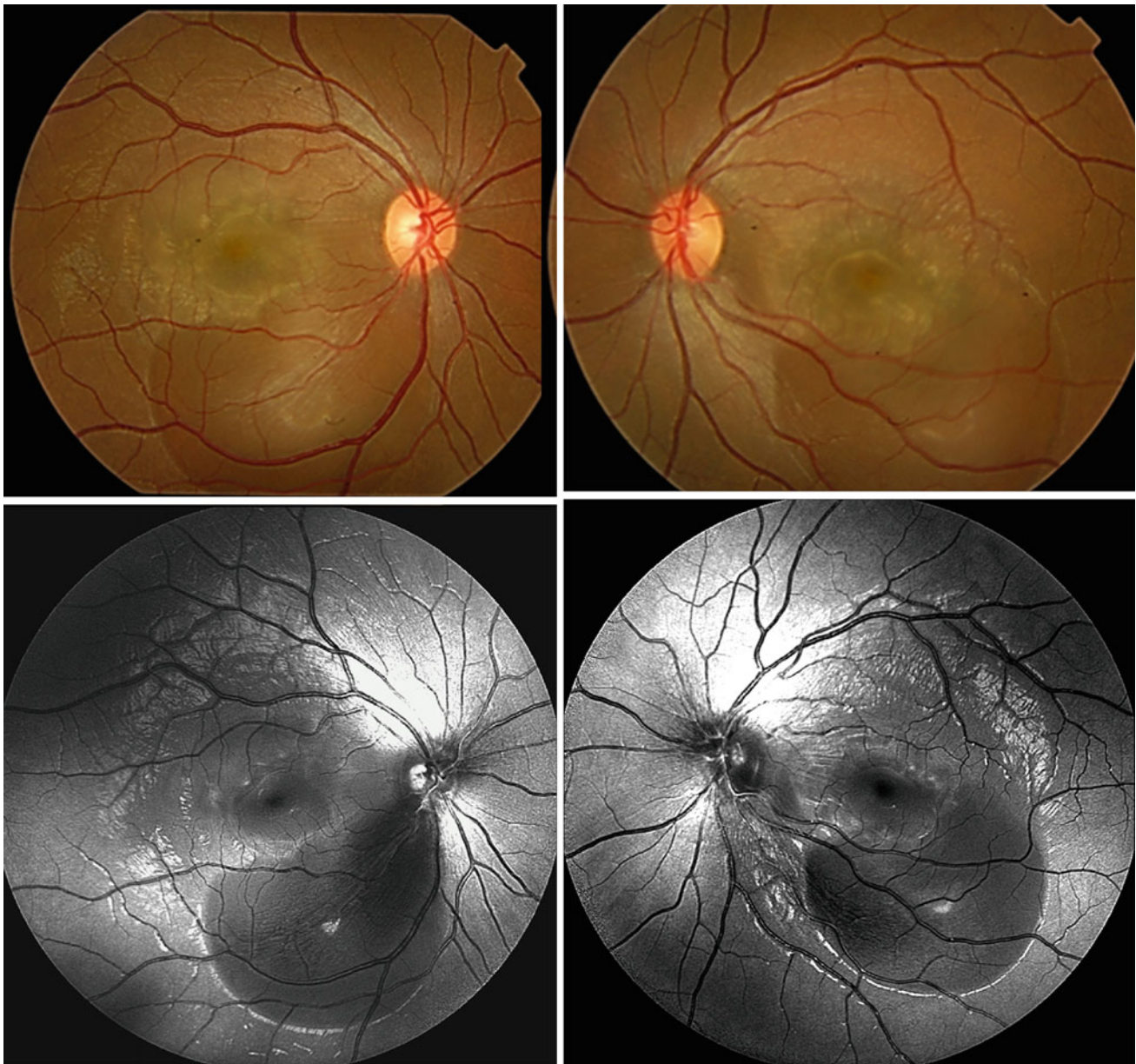
Fig. 10.8 Color fundus photographs and SLO images from a 19 year-old woman with decreased vision in both eyes and eye pain in the preceding 5 days with visual acuity of less than 20/160 in both eyes. Large serous detachment in both eyes at the inferior part of macula is remarkable. *SLO* scanning laser ophthalmoscopy

Bruch's membrane complex may be splitting in the membrane or a focal increase in hyperreflectivity. However, all of these signs are not unique or pathognomonic for the diagnosis of toxoplasma chorioretinitis [27].

During the healing phase, a scar forms that is characterized by a complete posterior vitreous detachment with retinal atrophy and relative focal choroidal hyperreflectivity (Figs. 10.21 and 10.22).

10.6 Serpiginous Choroiditis

In this disease, inflammation affects the RPE and choriocapillaris layer [28]. It classically emanates from around the optic nerve with villiform projections radiating centrifugally [29]. It typically has a relapsing–remitting course with new lesions often adjacent to older lesions [30].Each flare
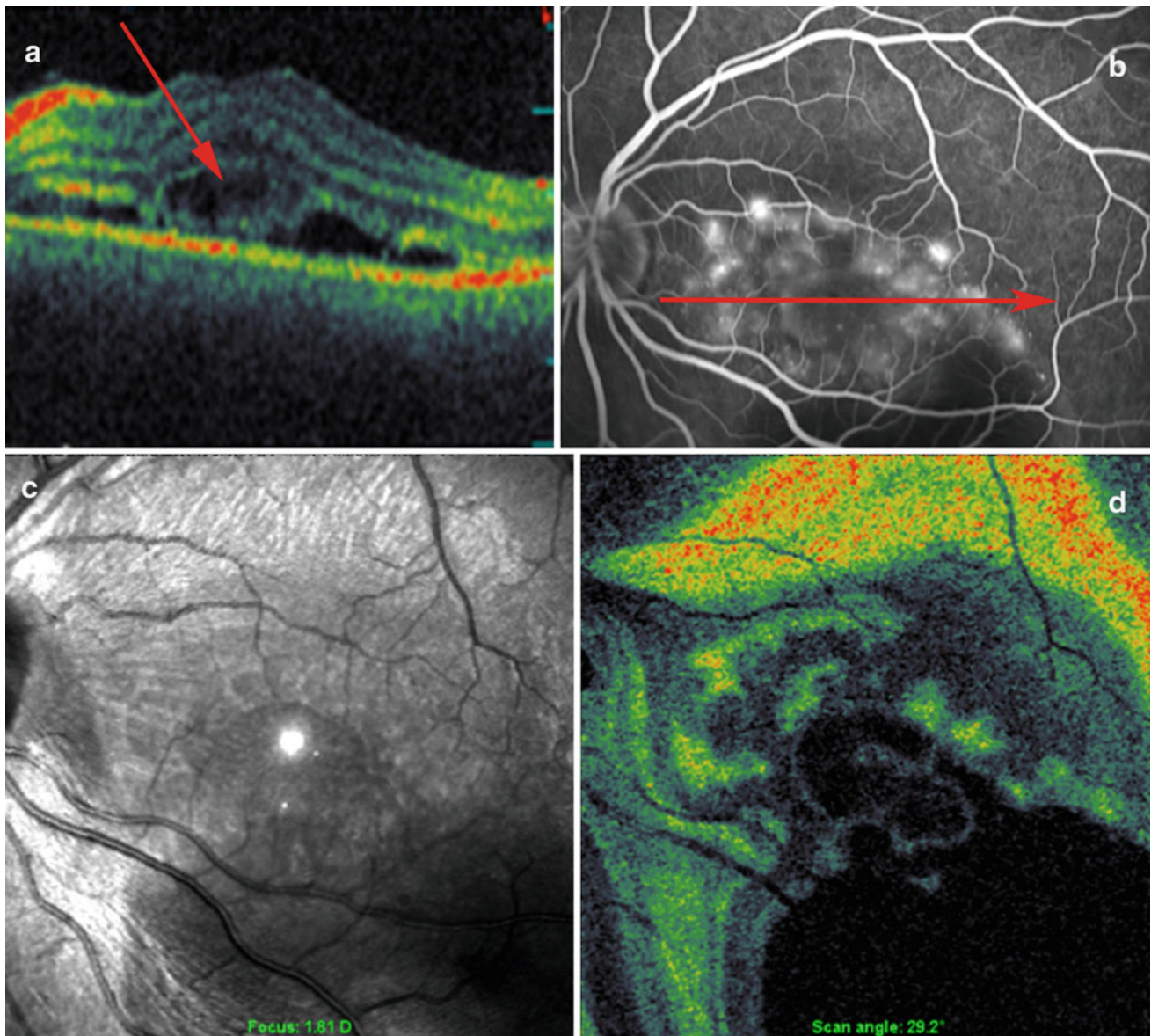
Fig. 10.9 **a** The cross-sectional time-domain (TD)-OCT image of the left macula of the patient in Fig. 10.8 shows intraretinal cystic changes and serous detachment. **b** The fluorescein angiography image shows the starry sky pattern with multiple hyperfluorescent dots that correspond to small serofibrinous detachments in the macula. **c** The SLO image shows retinal surface fine wrinkles that are associated with serous detachments and choroidal surface undulations. **d** The C-scan primarily cuts through the outer retinal surface and shows patchy columns (*patchy green areas*) at the outer aspect of the detached retina. OCT optical coherence tomography, SLO scanning laser ophthalmoscopy

encroaches close to the fovea, thereby endangering central vision. The anterior segment is typically quiet [31] (Figs. 10.23 and 10.24).

10.7 Multiple Evanescence White Dot Syndrome

Multiple evanescent white dot syndrome is a benign unilateral disease that is more common among young females. It has unique features in fundus autofluorescence and fluorescein and indocyanine green angiography (Figs. 10.25 and 10.26). Fluorescein angiography demonstrates an early hyperfluorescence (wreath-like pattern) and late staining of the white dot lesions.

The main OCT finding in multiple evanescence white dot syndrome (MEWDS) is disruption of the ellipsoid zone, which occasionally crosses the ELM and extends to the outer nuclear layer (ONL). Focal hyperreflective spicule-like lesions in the photoreceptor layer are another finding on OCT imaging of these patients, which corresponds to hypofluorescent lesions on ICG angiography (ICGA), and
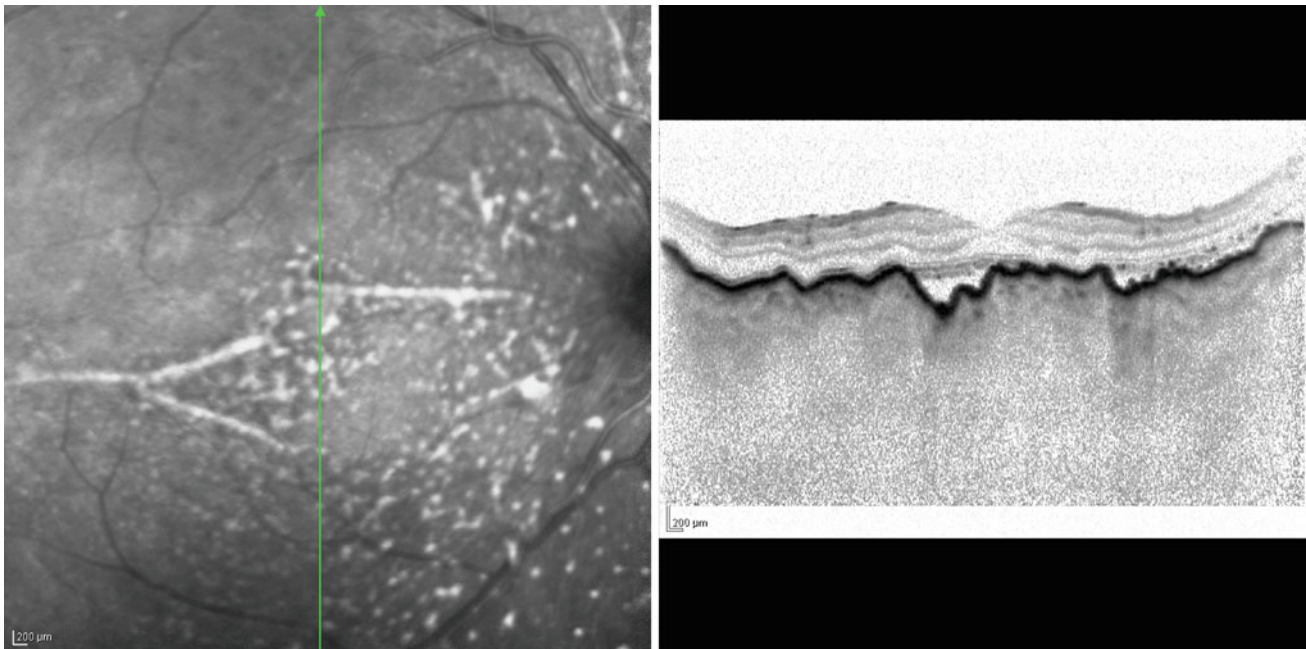
Fig. 10.10 The EDI-OCT and SLO images of a patient with active recurrent VKH disease. Choroidal homogeneity and the absence of the hyporeflective lumen of the choriocapillaris layer with multiple choroidal folds are evident. *EDI-OCT* enhanced depth imaging optical coherence tomography, *SLO* scanning laser ophthalmoscopy, *VKH* Vogt–Koyanagi–Harada

visual field defect on microperimetry. It has been hypothesized that these hyperreflective dots may result from damaged RPE cells leaking lipofuscin into the outer retinal layers [32]. Dome-shaped hyperreflectivity at the level of RPE, which may be disrupted outer segment, occurs in some patients. Granularity and nonspecific undulation of RPE have also been reported [33] (Fig. 10.27). In addition, thickening of subfoveal choroid may be present in EDI-OCT during the acute phase of MEWDS.

10.8 Acute Zonal Occult Outer Retinopathy

Acute zonal occult outer retinopathy (AZOOR) is a disease described by acute development of photopsia, scotoma and ERG abnormalities. It is more common in young female individuals. It affects the outer retina. Spectral-domain OCT (SD-OCT) imaging reveals attenuation and loss of the outer nuclear layer, ELM, ellipsoid zone, and interdigitation zone (cone outer segment tip) [34]. In severe cases, thinning of inner retina has been observed [35]. The central fovea will not be involved until the late stages. Disruption of the interdigitation line among the three hyperreflective bands of the outer retina in the zone of involvement is the most consistent finding and its recovery is associated with improvement on the electroretinogram (ERG) and in visual function [36]. When SD-OCT reveals loss of the outer nuclear layer, it is less likely that the photoreceptor outer segments recover because photoreceptor cell bodies are in the outer nuclear layer [37]. The location of diminished multifocal ERG and visual field defect and photopsia and outer retina defect are superimposed. In advanced cases, atrophy of the photoreceptors, RPE, and choroid can be seen (Figs. 10.28, 10.29, 10.30, 10.31, 10.32, 10.33, 10.34, 10.35, 10.36 and 10.37).

10.9 Multifocal Choroiditis with Panuveitis

The site of involvement in multifocal choroiditis with panuveitis is predominantly the outer retina and RPE. (Figs. 10.38, 10.39 and 10.40) Lesions composed of material with medium hyperreflectivity on OCT accumulate beneath the RPE. These RPE elevations usually have a conical shape, although some elevations with broader lateral dimensions may develop. Nevertheless, all elevations have a
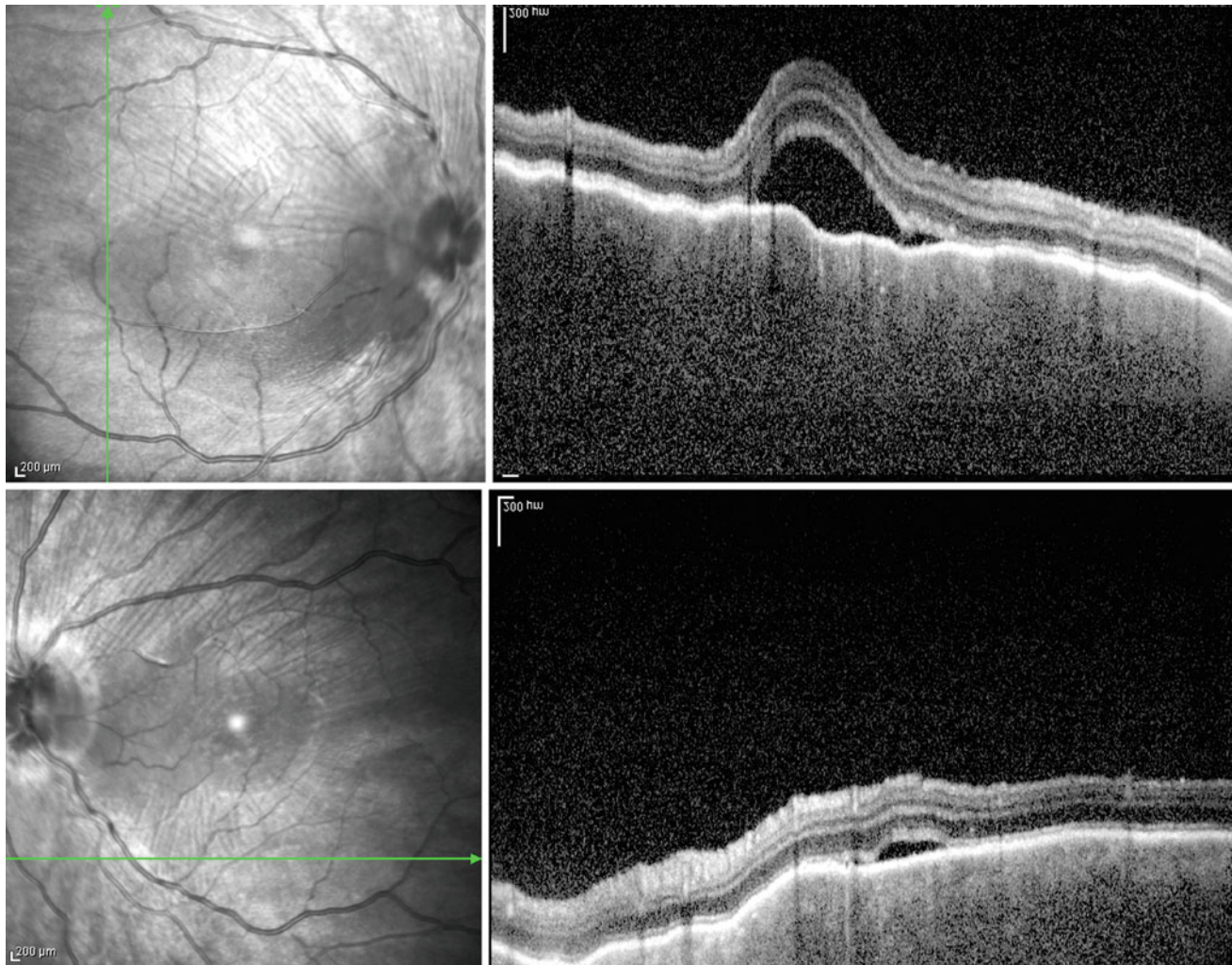
Fig. 10.11 The EDI-SLO-OCT images from the same patient in Fig. 10.6. Choroidal homogeneity and disappearance of the normal choriocapillary plexus and choroidal vessels lumens are evident. In addition, The OCT image of the fundus shows choroidal folds as dark and light striae radiating from the optic disc to the peripheral part. The RPE undulations are visible on OCT (*arrows*) and correspond to areas where the scan line intersects the choroidal folds. Inner limiting membrane wrinkling can be seen. *EDI* enhanced depth imaging, *OCT* optical coherence tomography, *RPE* retinal pigment epithelium, *SLO* scanning laser ophthalmoscopy

similar height. They may rupture and cause the material to infiltrate through the outer retina, which results in atrophy [38].

10.10 Presumed Mycobacterium Tuberculosis Choroiditis

Intraocular involvement of *Mycobacterium tuberculosis* (TB) can present in several ways: anterior uveitis (e.g., granulomatous type with high posterior synechia), vitritis, papillitis, retinitis, and retinal vasculitis, Eale's disease with peripheral occlusive retinal vasculitis, choroiditis, and multifocal serpiginoid choroiditis.

The primary site of involvement in ocular TB is the choroid in the form of focal or multifocal or serpiginous-like choroiditis, or solitary or multiple tuberculous granulomas. The inflammation may extend and affect the retina in the form of vasculitis or rarely granuloma formation [39].

Choroid granuloma presents as a choroidal elevation with an overlying focal adhesion between the choriocapillaris layer, RPE, and retina (i.e., contact sign). Subretinal fluid may exist around the choroid tubercle, although inflammation causes contact between these elements overlying the tubercle. The retina above the choroidal tubercle shows hyperreflectivity in the outer layers, most likely because of inflammatory infiltration [40] (Fig. 10.41).
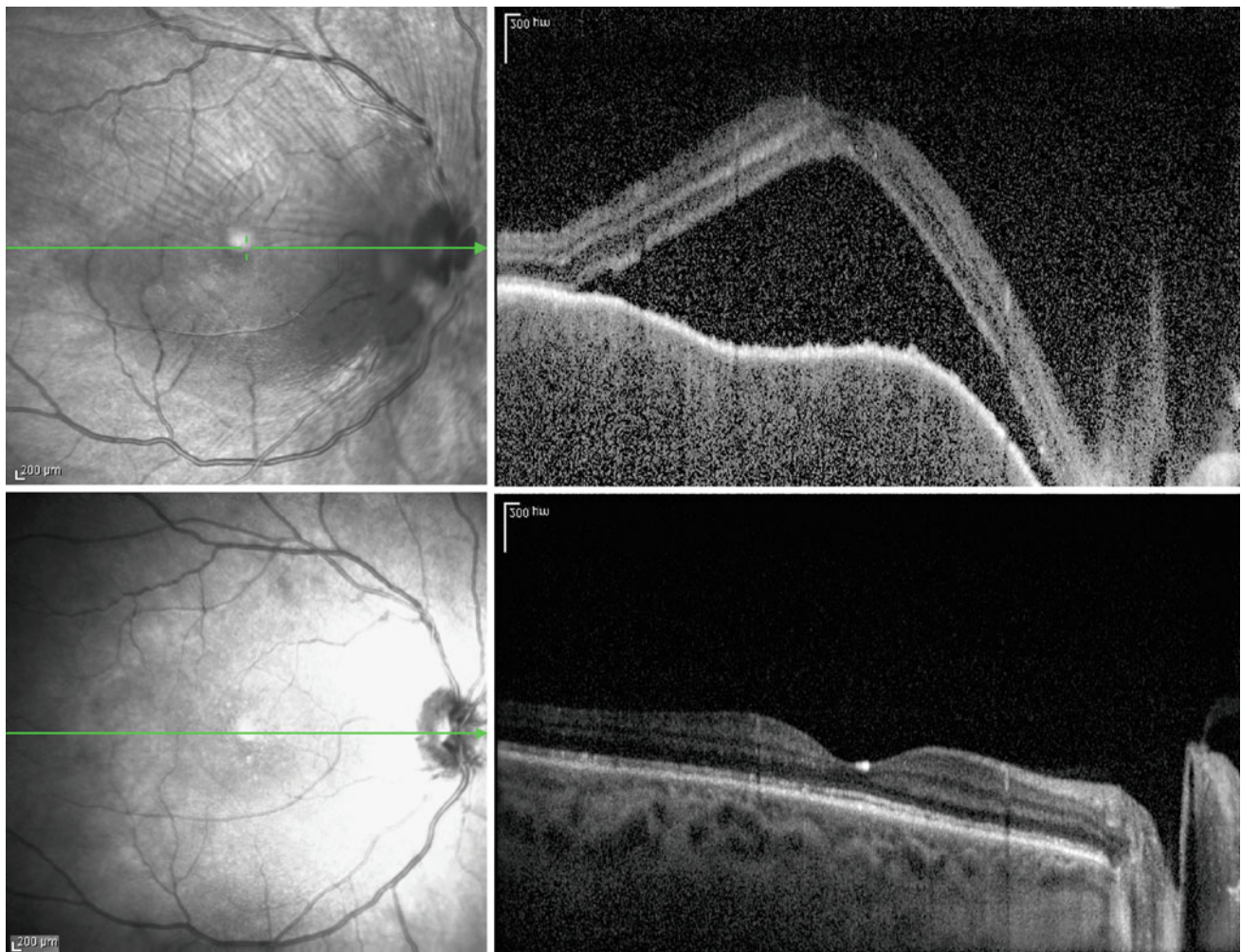
Fig. 10.12 These are EDI-SLO-OCT images of the right eye fovea of the patient in Fig. 10.6 at the acute stage of the disease (*upper image*) and after treatment (*lower image*). Loss of the normal choroidal vascular pattern and increased homogeneity of choroid occurs in the active phase of the disease. In the remission phase, choroidal homogeneity disappears and the normal architecture of choroidal plexus is restored. RPE undulation disappears as well. *EDI* enhanced depth imaging, *OCT* optical coherence tomography, *RPE* retinal pigment epithelium, *SLO* scanning laser ophthalmoscopy

The reason for decreased visual acuity is macular edema, which can develop in the form of diffuse, cystic, or serous retinal detachment. Serous retinal detachment is the most common form of macular edema in tuberculous uveitis [41] (Figs. 10.42 and 10.43).

Treatment with anti-TB drugs resolves the choroidal tubercle, which leaves a flat scar with shadowing [42] (Figs. 10.44 and 10.45).

10.11 Sarcoidosis

Sarcoidosis is a chronic idiopathic multisystem disorder characterized by non caseating epithelioid granuloma. Ocular sarcoidosis may involve any part of the eye including adnexa. Vitritis, intermediate uveitis, panuveitis, retinal vasculitis, and optic nerve involvement are among the posterior manifestations [43]. Iris nodule, posterior synechia and keratic precipitate are among the anterior manifestations. Sarcoid lesions may appear as retinal and pre-retinal granuloma (Lander's sign) or choroidal granuloma [44, 45]. Sarcoid granulomas are located in the stroma of the choroid and appear as multiple oval dull yellow lesions with a well-defined border. In EDI-OCT, they are hypo-reflective with no overlying RPE or retina changes, however, choriocapillaris attenuation can occur due to mass effect. In contrast, tubercular granuloma is solitary and lobulated with an intense yellow color. TB granulomas may be vascular with overlying hemorrhage and is accompanied with overlying outer retinal changes. Choroid is thickened at the site of granuloma [46] but, despite TB granuloma, does not cause retina elevation. Large granulomas are round-shaped,
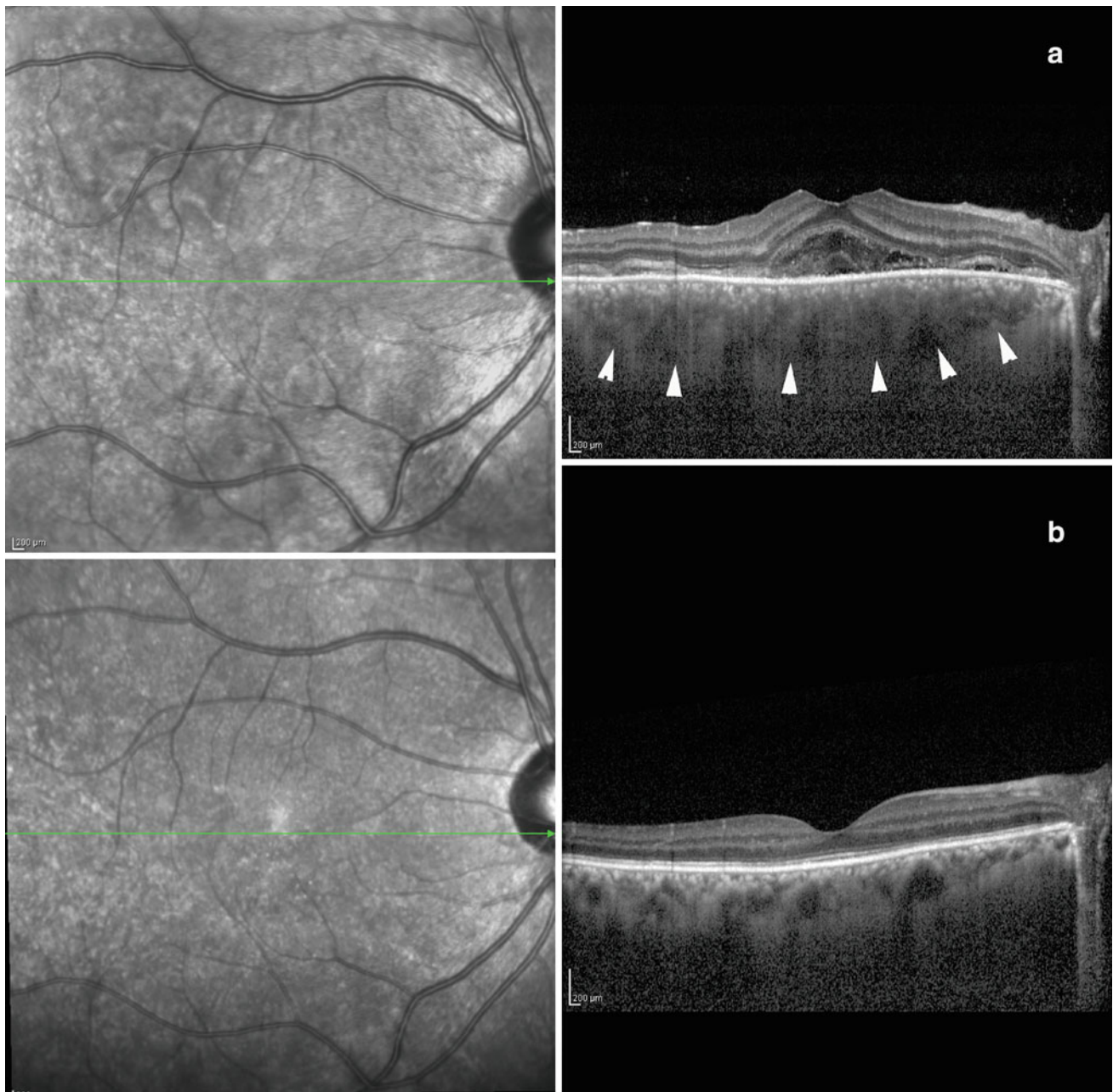
Fig. 10.13 **a** The EDI-OCT image of an eye in the acute phase of VKH disease. Choroidal thickening and some degree of homogeneity are remarkable. The outer border of the choroid is indicated by the arrowheads. **b** After treatment and in the resolution phase, choroidal thickening subsides and a hyporeflective choriocapillaris layer reappears. *EDI* enhanced depth imaging, *OCT* optical coherence tomography, *VKH* Vogt–Koyanagi–Harada

homogenous, and hypo-reflective lesions, while smaller ones are lobulated and non-homogenous [47, 48]. Sarcoid granuloma undergo an immediate decrease in size after successful treatment but homogeneity and hyporeflectivity may take longer to resolve. Following resolution, subretinal fibrosis and outer retinal tabulation ensue in the area of granuloma [49]. Additionally, It may present as infiltrative granulomatous lesion involving optic nerve head, characterized by swollen disc and hemorrhage. In case of optic nerve involvement, OCT scan shows granuloma as a highly
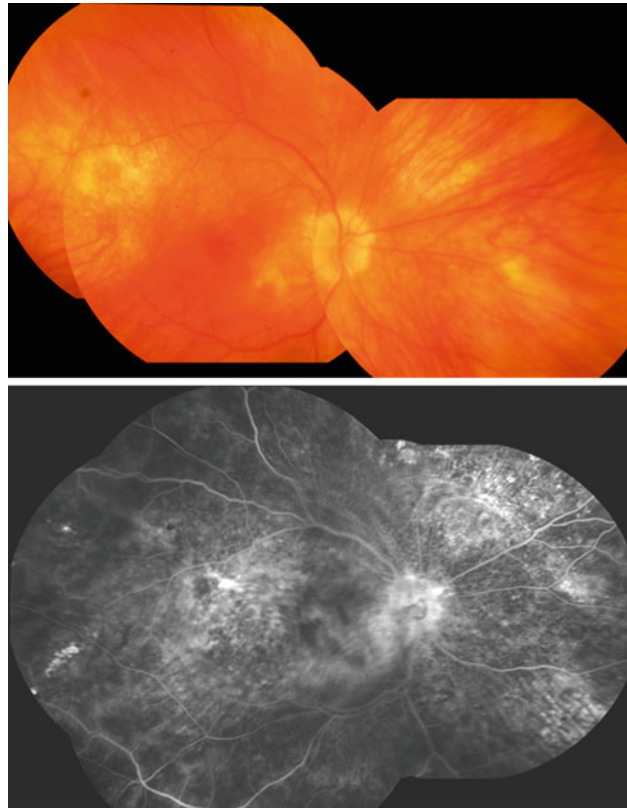
Fig. 10.14 Color fundus photograph and fluorescein angiography images of the right eye of a 41 year-old woman with an 18 year history of uveitis and 3 year history of vitiligo, with vision less than 20/200 in the right eye. Active recurrent disease results in depigmentation of the choroid and a sunset glow appearance

reflective lesion infiltrating the optic nerve head which can be nodular, accompanied by peripapillary intraretinal and subretinal fluid, and hyper-reflective intra-retinal dots suggesting an underlying inflammatory etiology. The choroid is also thickened [50].

10.12 Idiopathic Retinal Vasculitis, Aneurysms, and Neuroretinitis Disease

Idiopathic retinal vasculitis, aneurysms, and neuroretinitis (IRVAN) occurs more frequently in the female sex and around third decade of life [51]. There is no systemic association. Three major and three minor criteria exist for diagnosing this disease. Retinal vasculitis, saccular or fusiform aneurysmal dilation at the arterial division, and neuroretinitis are the major criteria; and peripheral capillary obstruction, macular exudation, and retinal neovascularization are the minor criteria. The disease is progressive and can cause severe visual loss and neovascular glaucoma. Visual prognosis depends on managing the ischemic retina before neovascularization develops [52] (Figs. 10.46, 10.47, 10.48, 10.49, 10.50 and 10.51).

10.13 Candida Endogenous Endophthalmitis

Fungi may be inoculated into the eye at the time ocular trauma (exogenous), or they may reach ocular tissue following hematogenous spread of a systemic infection (endogenous). Candida, a common normal flora of the human body may be pathogenic in certain circumstances, especially in immunocompromised patients. Whether reaching the eye through choroidal vessels (the most common route) or retinal
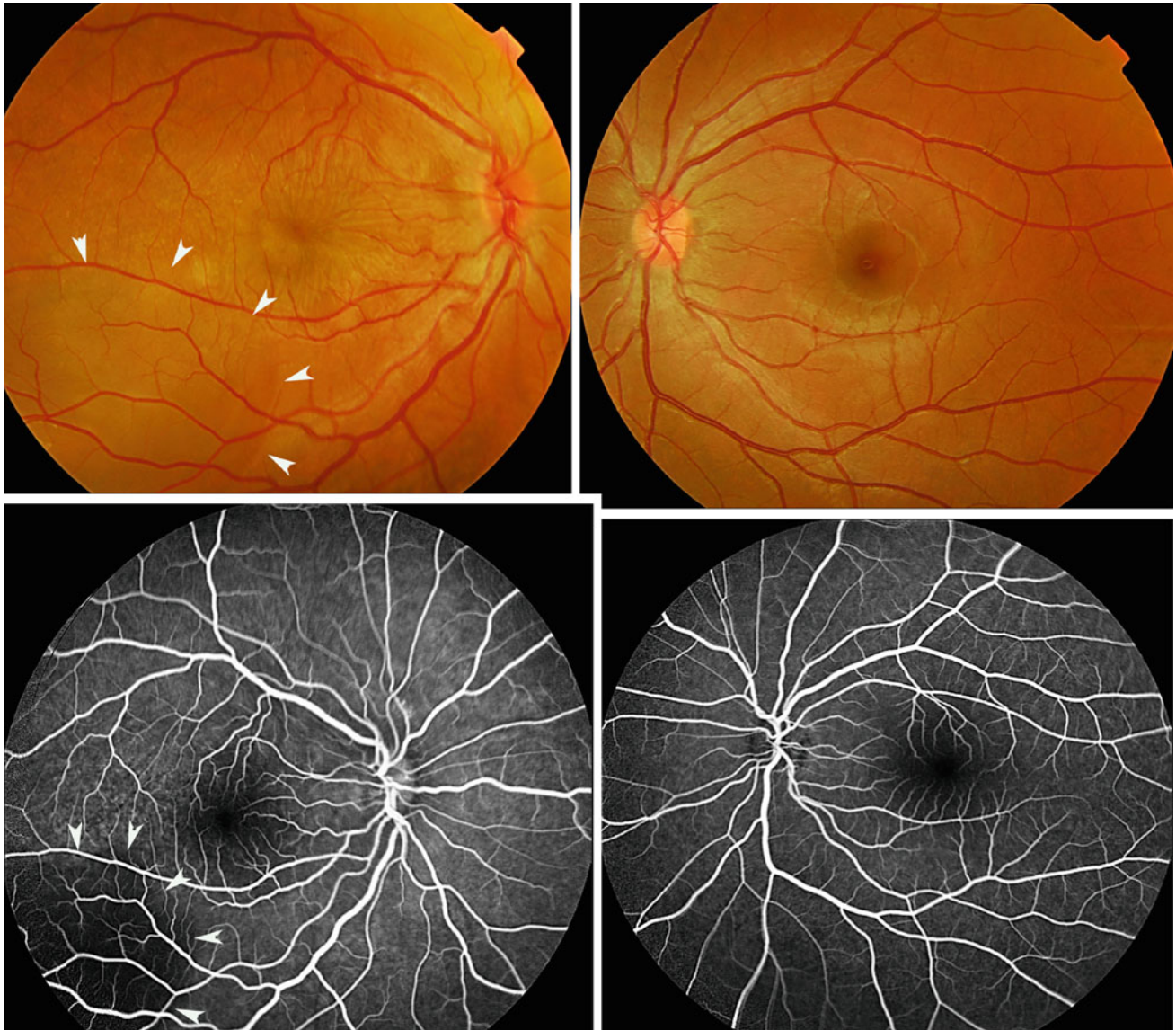
Fig. 10.15 Color fundus photograph and fluorescein angiography images from a 25 year-old woman with sudden severe pain and decreased vision in the right eye. The BCVA was 20/160 (OD) and 20/20 (OS). The slit lamp examination was unremarkable. Retinal ophthalmoscopy revealed extensive, multifocal serous detachment. Fluorescein angiography of the posterior pole was unremarkable, except for hypofluorescence at the area of serous detachment (*white arrowheads*). *BCVA* best corrected visual acuity, *OD* oculus dexter, *OS* oculus sinister
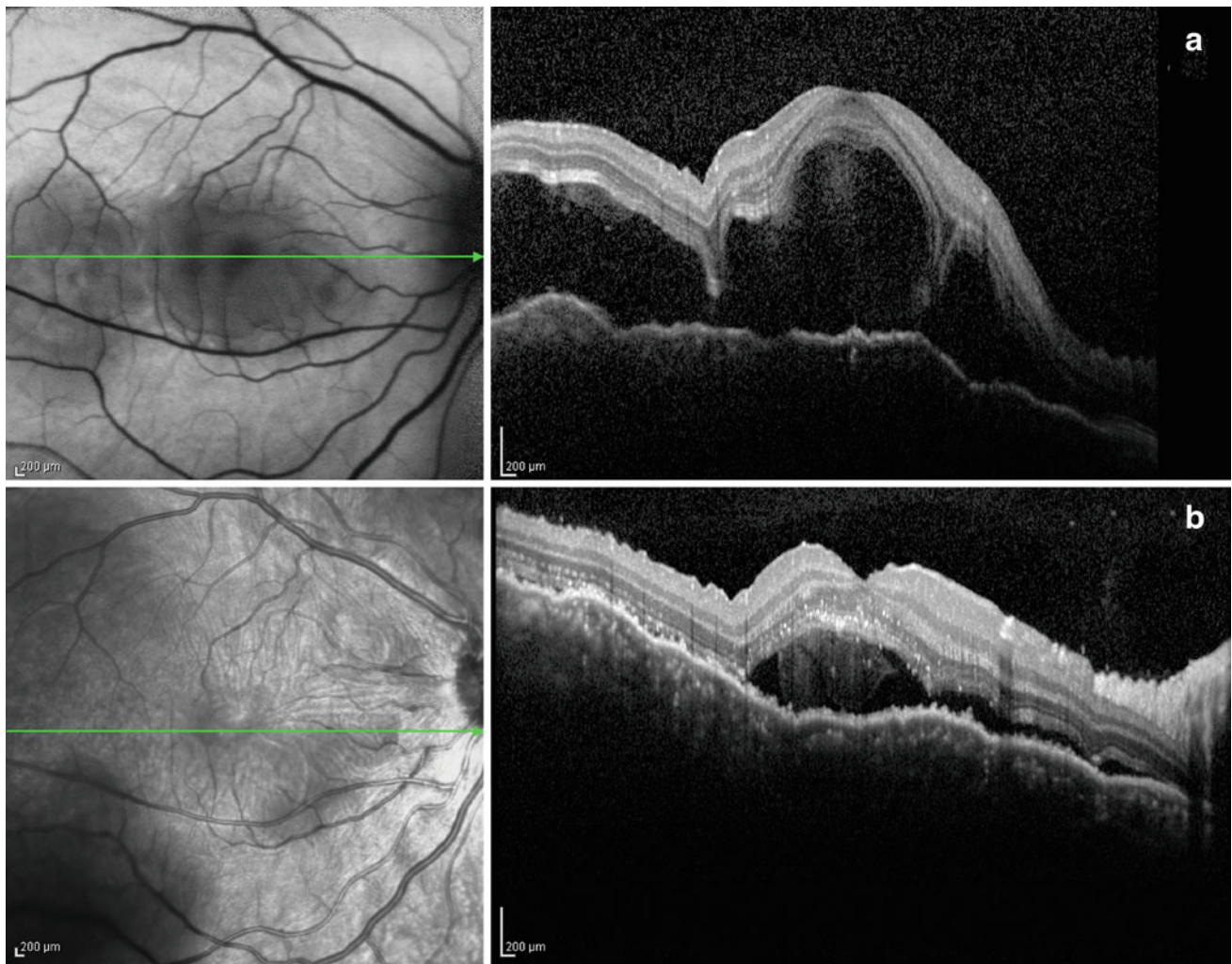
Fig. 10.16 **a** The FAF-OCT scan of the right eye (the same patient in Fig. 10.15) crosses the central fovea and shows multiple serous detachments with subretinal fibrin deposits and choroidal wrinkling that resemble the findings of VKH disease. Hyporeflective areas on the FAF image correspond to areas of serous retinal detachment. **b** The SLO-OCT image, obtained 5 days after high dose oral steroid therapy, illustrates decreased subretinal fluid, which was correlated to a visual gain (20/40). *FAF-OCT* fundus autofluorescence optical coherence tomography, *SLO-OCT* scanning laser ophthalmoscopy optical coherence tomography, *VKH* Vogt–Koyanagi–Harada
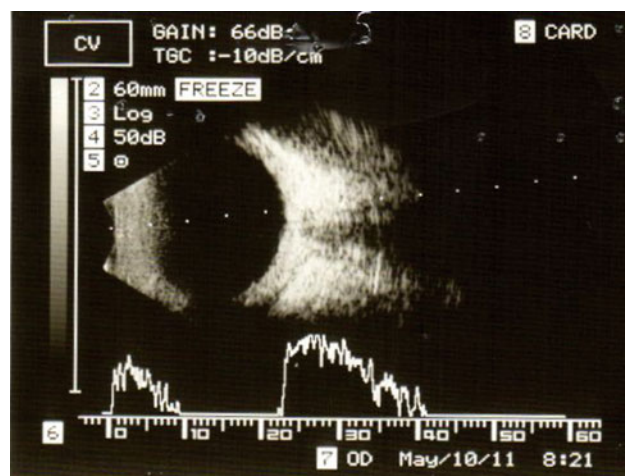

Fig. 10.17 The B-scan ultrasonography image of the right eye (the same patient in Fig. 10.15) demonstrates choroidal and scleral thickening

FIXATION MONITOR: BLIND SPOT
FIXATION TARGET: CENTRAL
FIXATION LOSSES: 0/12
FALSE POS ERRORS: 0 %
FALSE NEG ERRORS: 2 %
TEST DURATION: 03:46

FOVEA: OFF

STIMULUS: III, WHITE
BACKGROUND: 31.5 ASB
STRATEGY: SITA-FAST

PUPIL DIAMETER: 4.9 MM
VISUAL ACUITY:
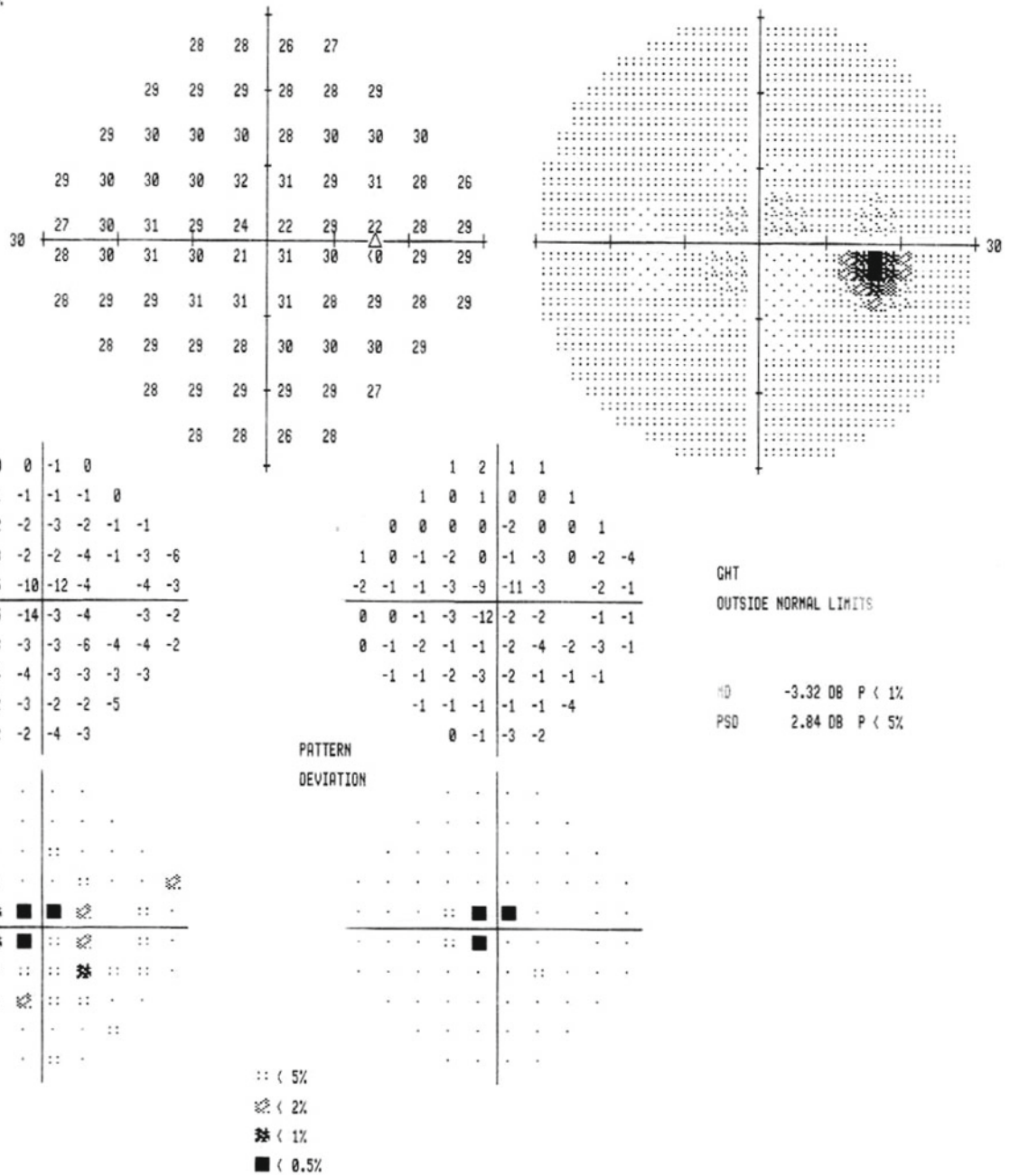RX: +0.00 DS   DC X

DATE: 05-09-2011
TIME: 13:10
AGE: 25

```
            28  28 | 26  27
        29  29  29 + 28  28  29
    29  30  30  30 | 28  30  30  30
  29  30  30  30  32 | 31  29  31  28  26
  27  30  31  29  24 | 22  29  22  28  29
30 +
  28  30  31  30  21 | 31  30  <0  29  29
  28  29  29  31  31 | 31  28  29  28  29
      28  29  29  28 | 30  30  30  29
          28  29  29 + 29  29  27
              28  28 | 26  28
```

TOTAL DEVIATION
```
        0   0  -1   0
    -1  -1  -1  -1  -1   0
  -2  -2  -2  -2  -3  -2  -1  -1
-1  -2  -2  -3  -2  -2  -4  -1  -3  -6
-3  -2  -3  -5 -10 -12  -4      -4  -3
-2  -2  -3  -5 -14  -3  -4      -3  -2
-2  -2  -4  -3  -3  -3  -6  -4  -4  -2
  -2  -3  -4  -4  -3  -3  -3  -3
    -2  -2  -3  -2  -2  -5
        -2  -2  -4  -3
```

PATTERN DEVIATION
```
            1   2   1   1
        1   0   1   0   0   1
      0   0   0   0  -2   0   0   1
  1   0  -1  -2   0  -1  -3   0  -2  -4
 -2  -1  -1  -3  -9 -11  -3      -2  -1
  0   0  -1  -3 -12  -2  -2      -1  -1
  0  -1  -2  -1  -1  -2  -4  -2  -3  -1
   -1  -1  -2  -3  -2  -1  -1  -1
     -1  -1  -1  -1  -1  -4
         0  -1  -3  -2
```

GHT
OUTSIDE NORMAL LIMITS

MD   -3.32 DB P < 1%
PSD   2.84 DB P < 5%

:: < 5%
⬗ < 2%
⬔ < 1%
■ < 0.5%

Fig. 10.18 Perimetry of the involved eye (the same patient in Fig. 10.15) reveals mild generalized depression and a deep small central scotoma
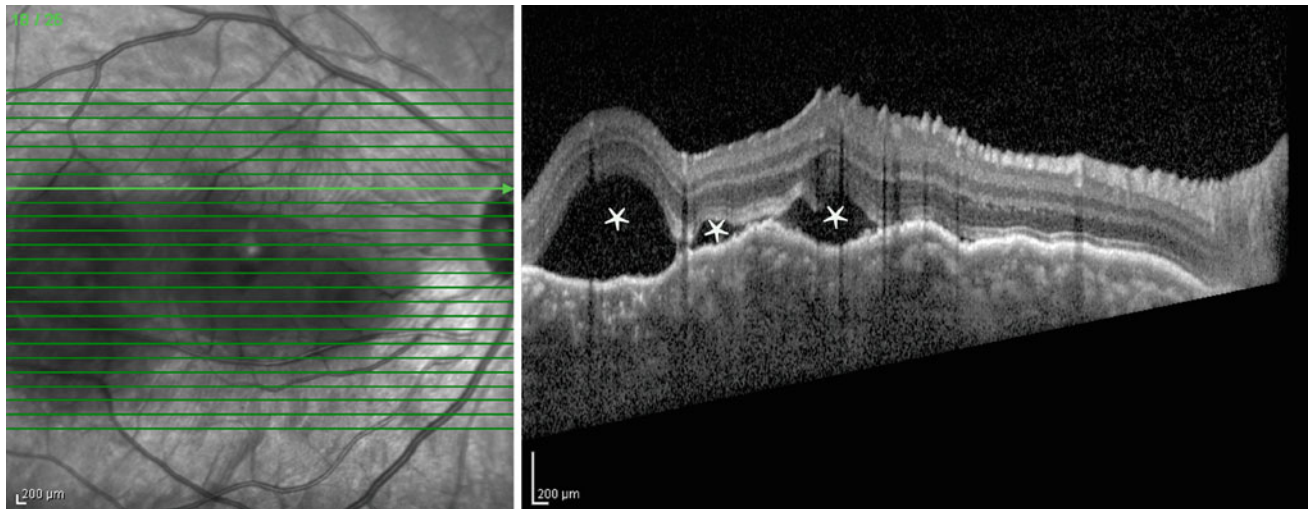
Fig. 10.19 The EDI-OCT image at the acute stage of the disease (the same patient in Fig. 10.15). Multiple serous detachments (*asterisks*) with multiple choroidal folds and retinal thickening are similar to the findings of VKH disease. Imaging by EDI-OCT and fluorescein angiography are key for differentiating this disease from VKH. Mild choroidal thickening and near-normal choroidal vasculature with open vascular lumens in the Haller and Sattler layer indicate minimal choroidal involvement. These findings accompanied by the lack of pinpoint leakage in fluorescein angiography are helpful in ruling out VKH syndrome. *EDI* enhanced depth imaging, *OCT* optical coherence tomography, *SLO* scanning laser ophthalmoscopy, *VKH* Vogt–Koy-anagi–Harada

circulation, fungal particles tend to accumulate on retinal surface, where they can reach vitreous body as the perfect milieu for growth [53]. The colonies of candida can be appreciated as white hyper-reflective round shaped homogenous lesions on the posterior retina which extend into vitreous cavities. The highly reflective pre-retinal lesions cast a shadow on the underlying retinal tissue. The combination of white lesion and posterior dark shadow is called "raincloud" sign [54].
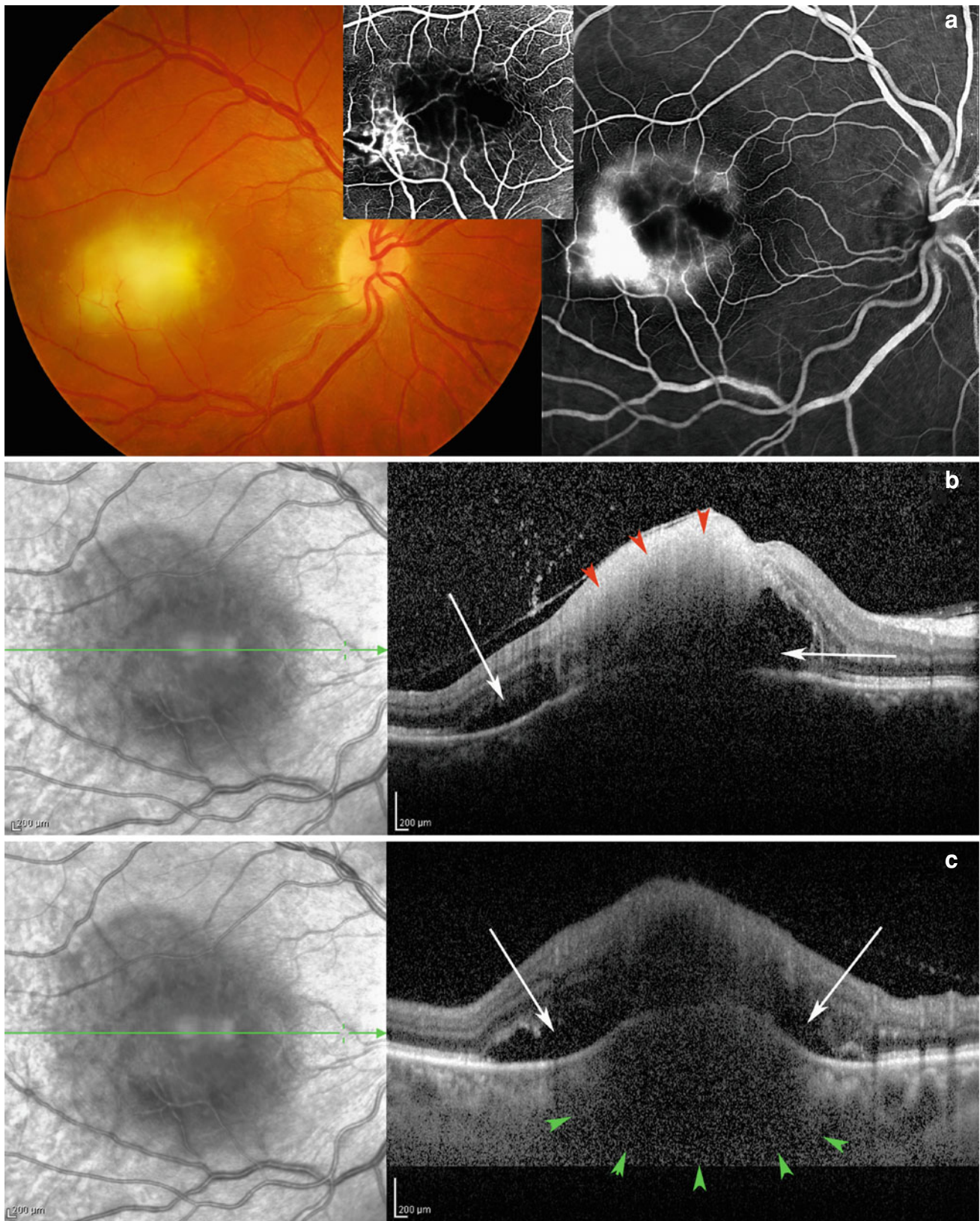
Fig. 10.20 The fundus photograph, fluorescein angiography, and SLO-OCTs and EDI-OCT images of a patient in the active phase of toxoplasmosis retinochoroiditis. Perifoveal vascular occlusion is apparent in arteriovenous phase of angiography (inset). **a** The retina is thickened by a full-thickness homogenous hyperreflective lesion (*red arrowheads*), which represents severe retinitis of ocular toxoplasmosis. **b** Hyporeflective spaces around the lesion are subretinal fluid (*white arrows*). The posterior hyaloid is attached to the lesion and is thickened. Hyperreflective deposits are also visible in the vitreous adjacent to the lesion. In addition, several small round hyperreflective spots are on the vitreoretinal surface adjacent to the lesion. **c** In the EDI-OCT image, choroidal granuloma and inflammation (*green arrowheads*) push the RPE layer upward and represent the choroiditis component of ocular toxoplasmosis. EDI enhanced depth imaging, OCT optical coherence tomography, RPE retinal pigment epithelium, SLO scanning laser ophthalmoscopy
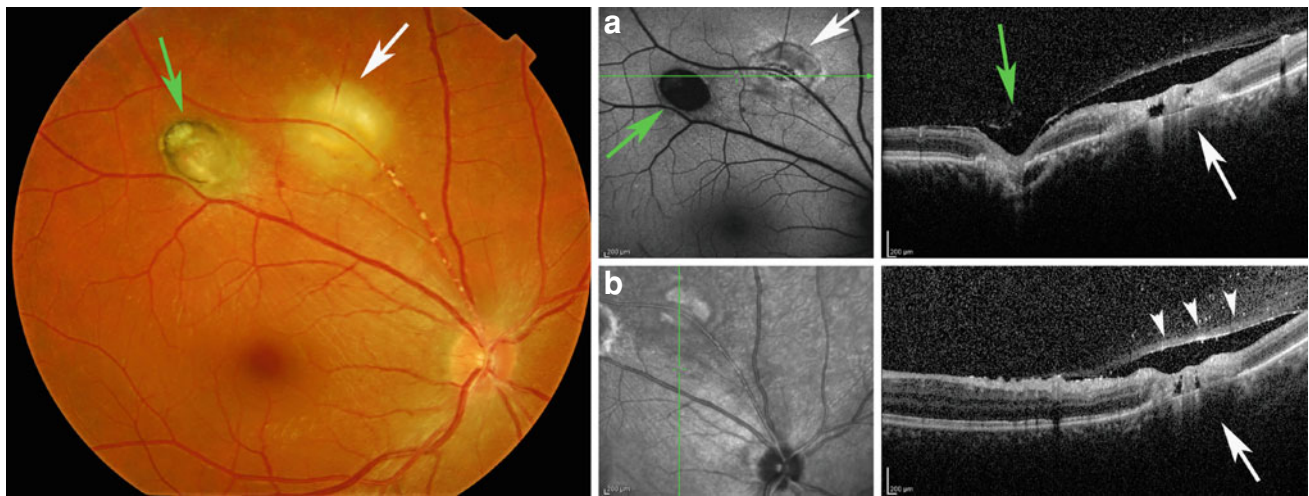
Fig. 10.21 The color fundus photograph and FAF and SLO-OCT images from a patient with active recurrent ocular toxoplasmosis. The green arrows indicate the old scar from a previous inflammation. **a** In the FAF image, hyporeflectivity in that area represents loss of the RPE, retina, and choroid. In the partially active lesion (*white arrows*), full-thickness retinal involvement with loss of definition of layers and tissue destruction with cyst-like spaces are evident. **b** On OCT, vitreous infiltration and inflammation over the involved area are evident (*white arrowheads*). FAF fundus autofluorescence, OCT optical coherence tomography, RPE retinal pigment epithelium, SLO scanning laser ophthalmoscopy
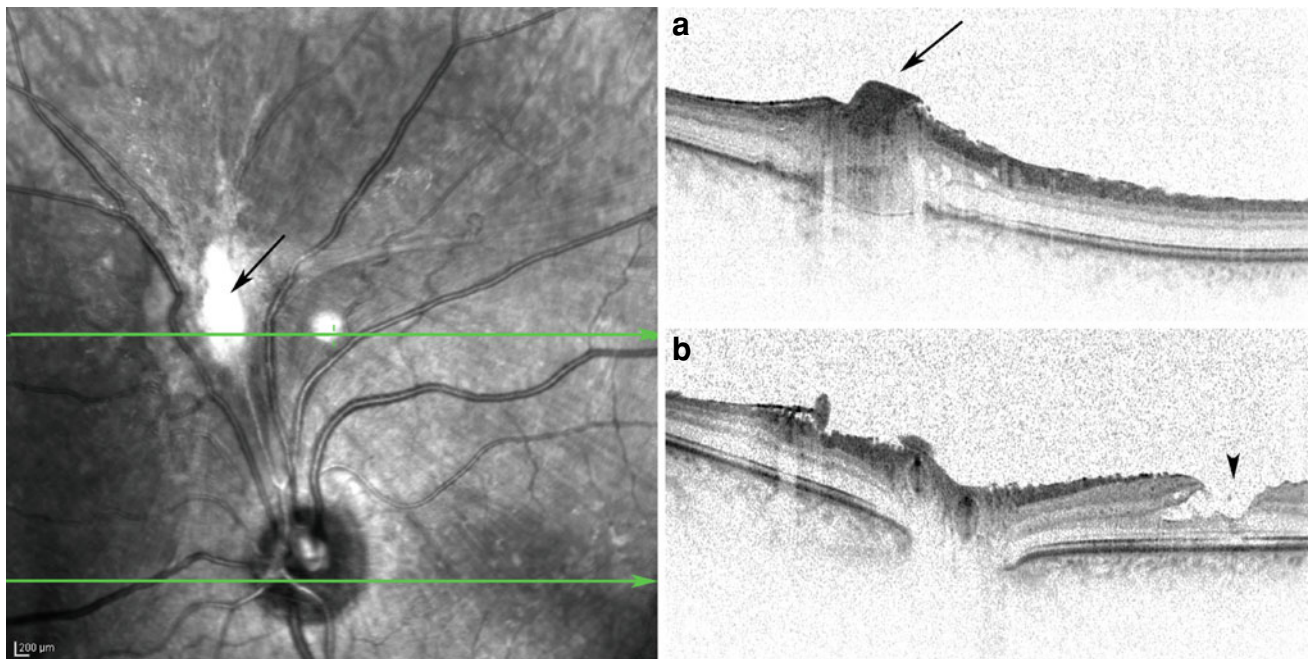
Fig. 10.22 The two cross-sectional OCT scans pass through the previous retinitis and scar area (section a) and the optic disc and fovea (section b). **a** The hypertrophied scar involves all retinal layers, Bruch's membrane, and the choroidal layer (*black arrow*). **b** Exudation results in the formation of an epiretinal membrane and subsequent retinal wrinkling that eventually causes a lamellar macular hole and cleft (*black arrowhead*). *OCT* optical coherence tomography
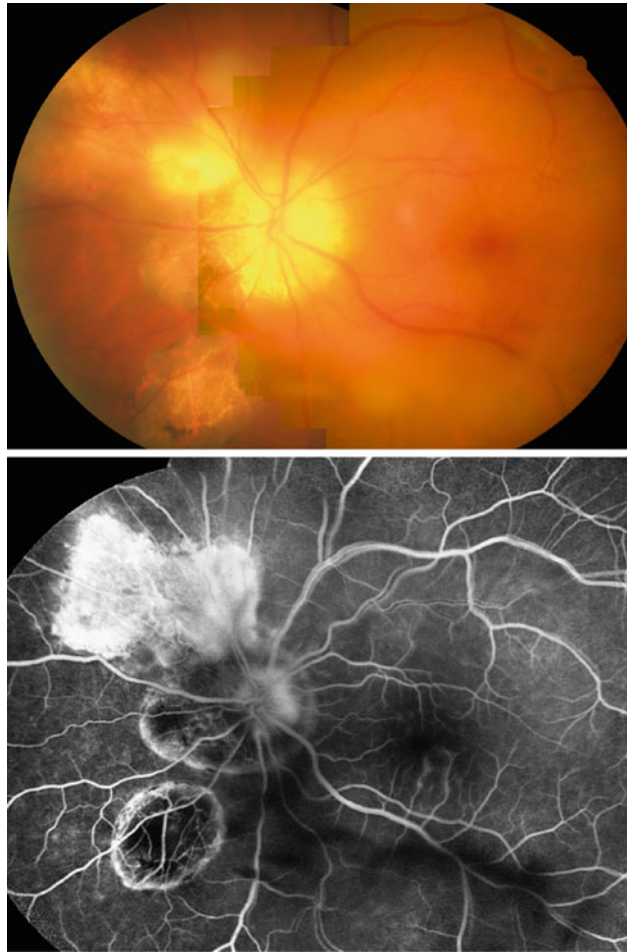
Fig. 10.23 A 59 year-old woman with a 30 year history of gradual vision disturbances with floaters in the left eye. She experienced several episodes of exacerbation and remission, and required the administration of systemic corticosteroid to control symptoms. Visual acuity is 20/25. Chorioretinal scars in peripapillary area with extension to periphery are evident. FA in the late phase show an active lesion superonasal to the optic nerve that has considerable leakage with localized exudates to the adjacent vitreous
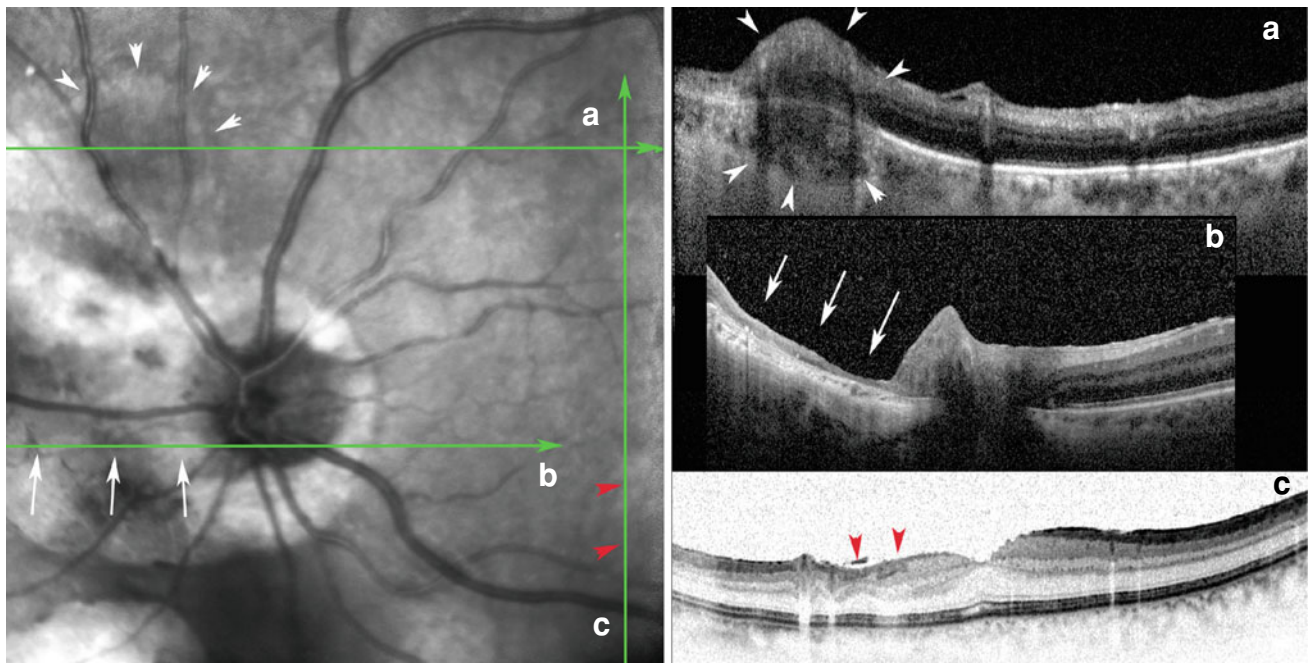
Fig. 10.24 The EDI-OCT images from the same patient in Fig. 10.23. **a** The cross-section of active lesion reveals edema of the choroid and overlying retina (*white arrowheads*). **b** The scar area shows near total retinochoroidal loss (white arrows). **c** A vertical scan through the central foveal shows thinning of the inferior parafoveal area with nerve fiber layer loss that corresponds to the area of perifoveal vasculitis (*red arrowheads*). *EDI-OCT* enhanced depth imaging optical coherence tomography
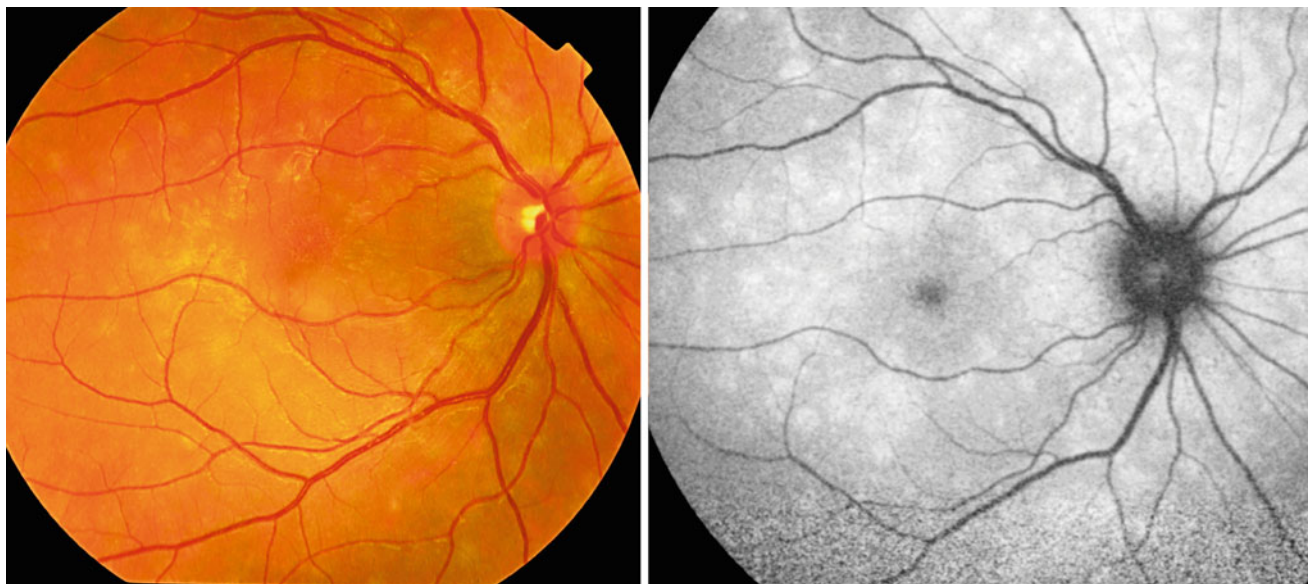
Fig. 10.25 Color fundus photograph and fundus autofluorescence image from a patient with the diagnosis of MEWDS. Fundoscopy of the contralateral eye is normal. Multiple white patches are mostly distributed around optic disc in the fundus photograph and appear as hyperautofluorescent patches in the FAF images. *FAF* fundus autofluorescence, *MEWDS* multiple evanescence white dot syndrome
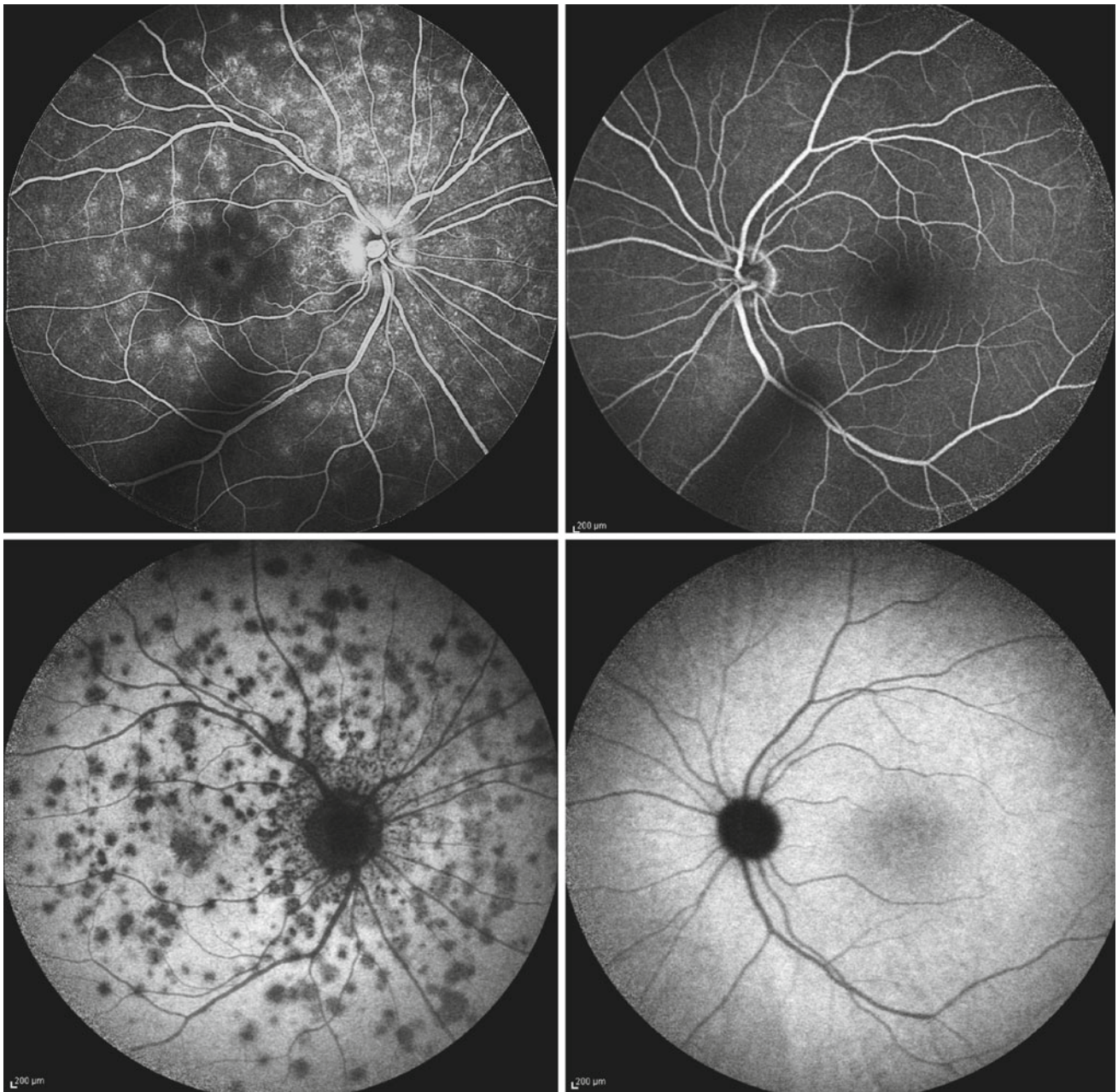
Fig. 10.26 Late phase of fluorescein angiography and indocyanine angiography of the same patient in Fig. 10.25. Dot lesions in MEWDS reveal staining on the fluorescein angiography image and hypocyanescence on the ICG angiography image. *ICG* indocyanine green, *MEWDS* multiple evanescence white dot syndrome
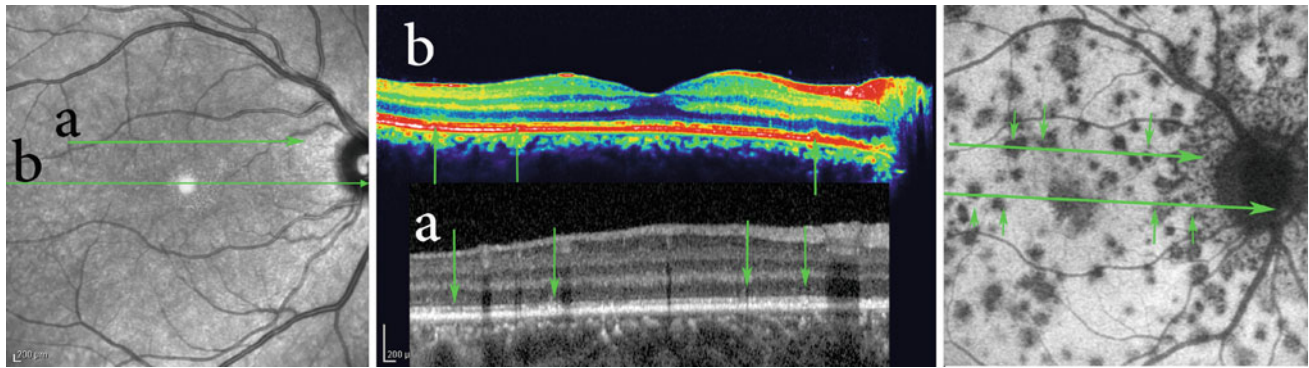
Fig. 10.27 The SLO-OCT image of the same patient in Fig. 10.26 shows two horizontal sections. Small foci of disruption in the ellipsoid zone match the hypofluorescent areas on ICGA (small *green arrows*). Focal hyperreflective lesions are visible in the photoreceptor layer. *ICGA* indocyanine green angiography, *SLO-OCT* scanning laser ophthalmoscopy optical coherence tomography

Fig. 10.28 Color fundus photographs and fluorescein angiography images from a 30 year-old woman with recent decreased vision in both eyes (OD is 20/200 and OS is 20/500). The fundus of both eyes is unremarkable (*upper images*). In fluorescein angiography (*lower image*), mild late optic disc hyperfluorescence with some hypofluorescent dots under the retina exist in both eyes. Inferior arcade vasculitis is evident in the right eye. *OD* oculus dexter, *OS* oculus sinister
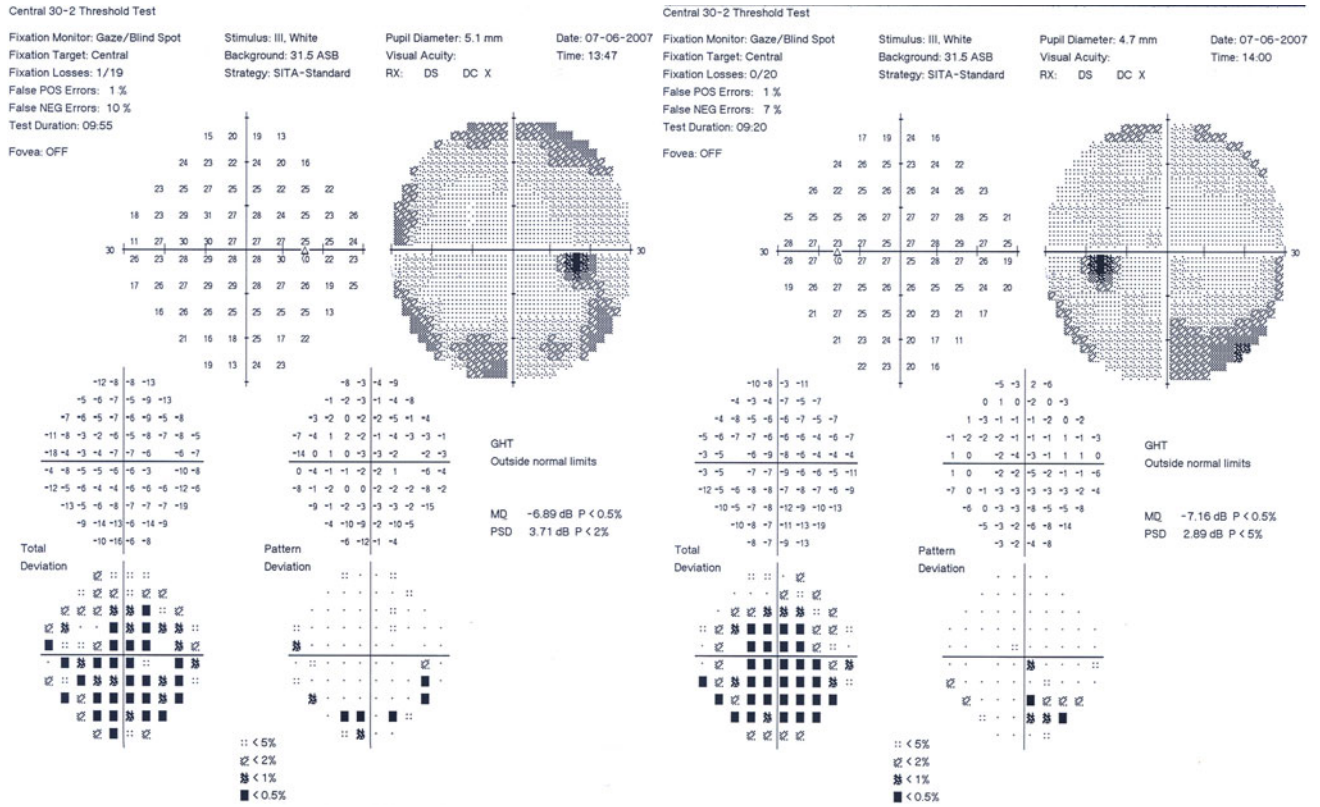
Fig. 10.29 Humphrey visual field findings of both eyes (the same patient in Fig. 10.28) reveal nonspecific visual field loss in both eyes
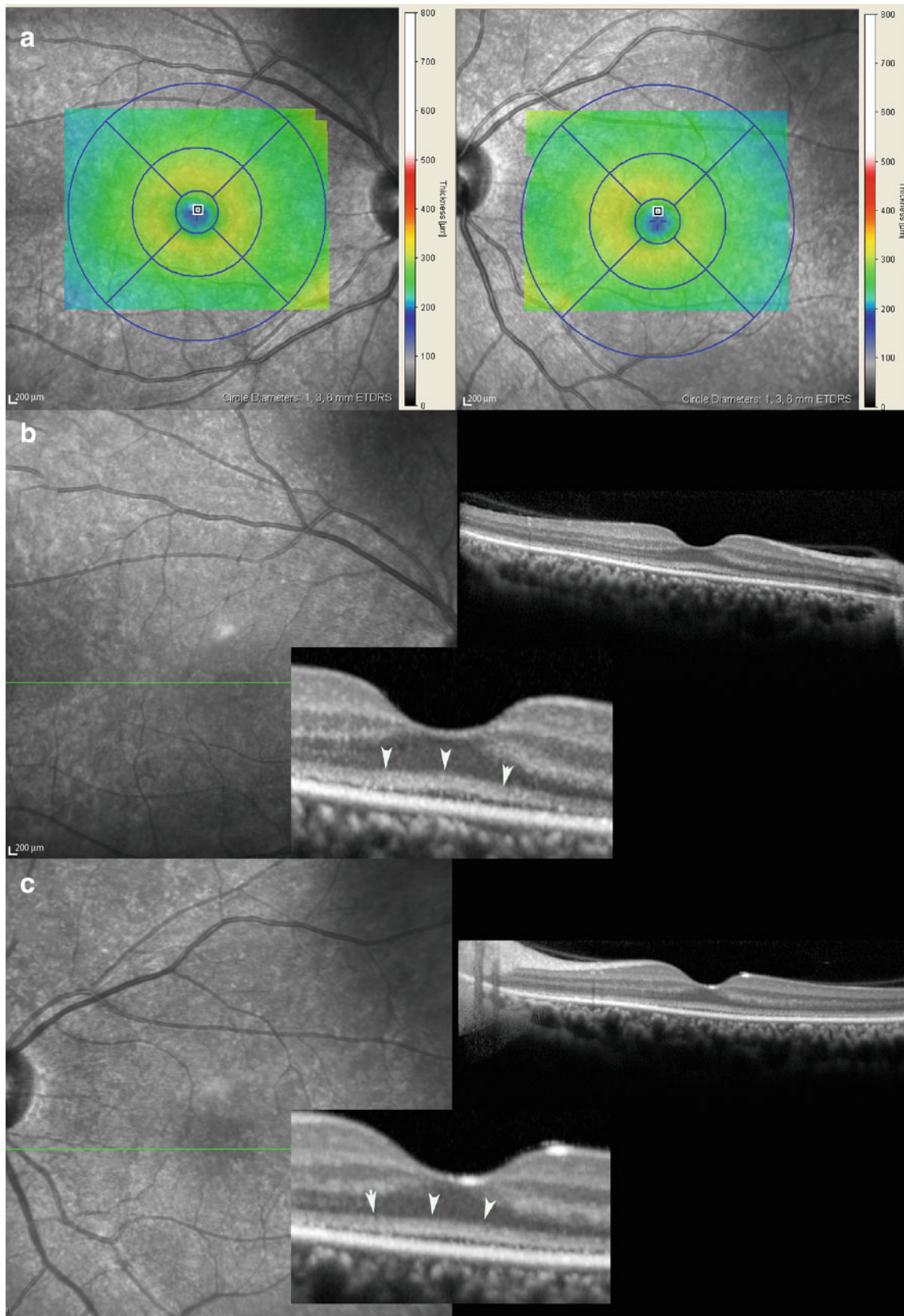
Fig. 10.30 The SLO-OCT image of both eyes of the same patient in Fig. 10.28 shows that the external limiting membrane and ellipsoid zone and interdigitation zone (cone outer segment tip) are less distinct (white arrowheads). This defect is more prominent in areas away from the fovea. *SLO-OCT* scanning laser ophthalmoscopy optical coherence tomography
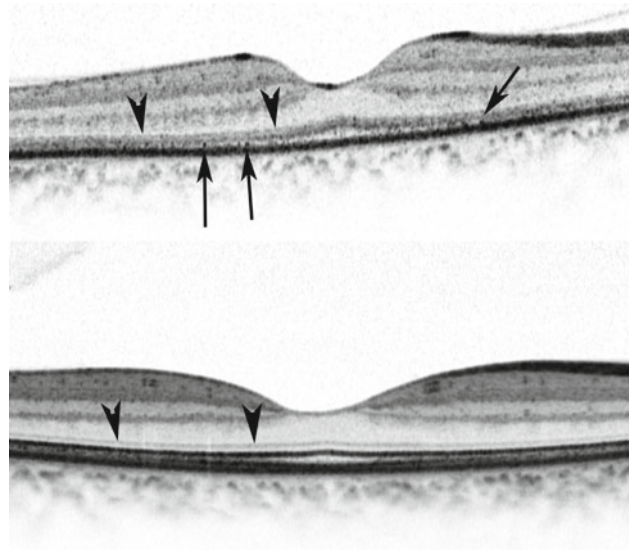
Fig. 10.31 Differences between outer retinal layers (*arrowheads*) in a patient with AZOOR (*upper image*) and a normal person (*lower image*). In AZOOR, multifocal subretinal deposits are visible on an SD-OCT image (*arrows*). Derangement of the outer retina is also visible. Fovea is relatively spared. *AZOOR* acute zonal occult outer retinopathy, *SD-OCT* spectral-domain optical coherence tomography
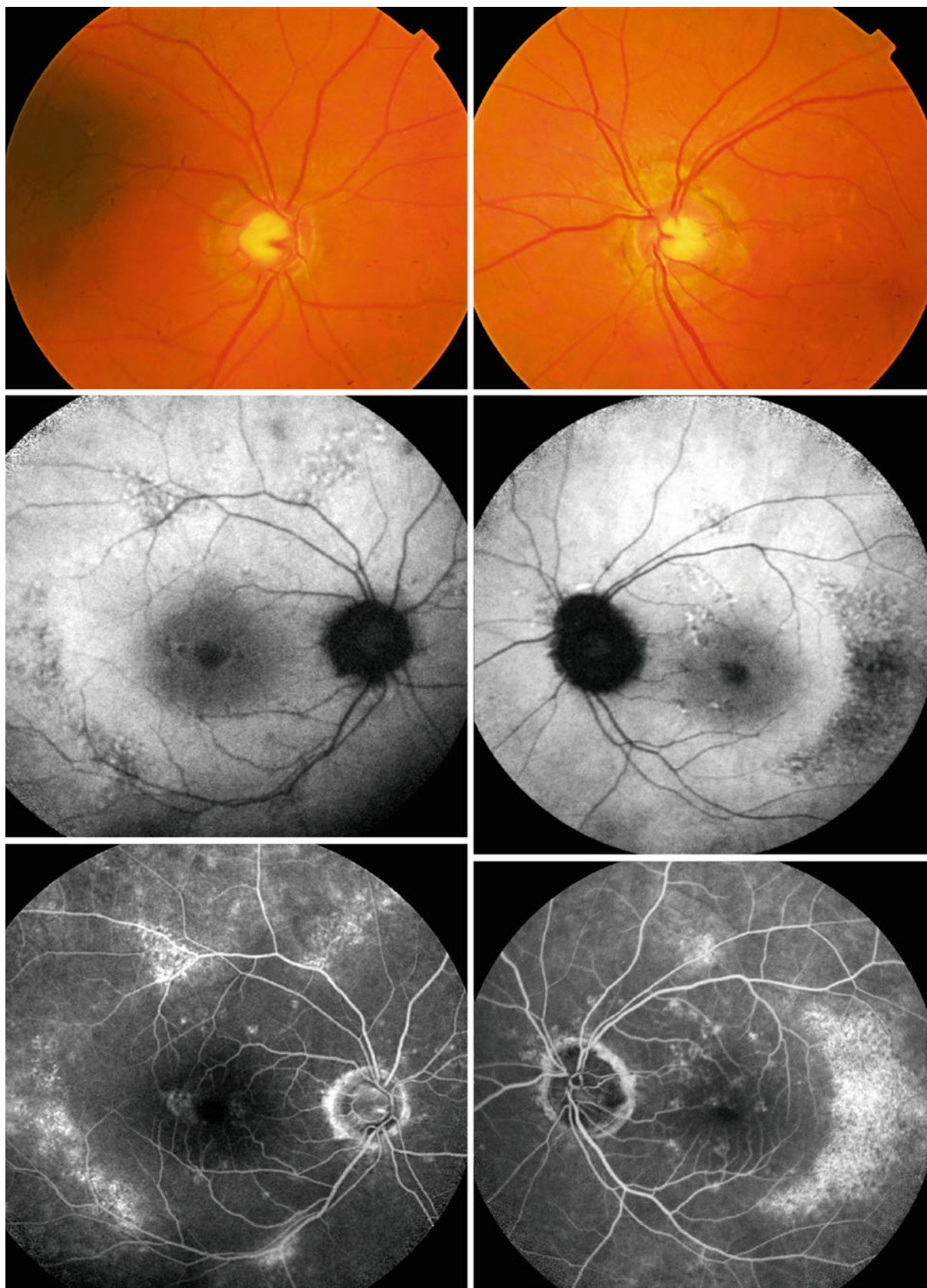
Fig. 10.32 Color fundus photographs and FAF and fluorescein angiography images from a 61 year-old man with a history of progressive field defect. The fundus and FAF images reveal classic peripapillary hypofluorescence secondary to RPE atrophy. The FA image reveals peripapillary hyperfluorescence and perivascular leakage. *FA*, fluorescein angiography, *FAF* fundus autofluorescence, *RPE* retinal pigment epithelium
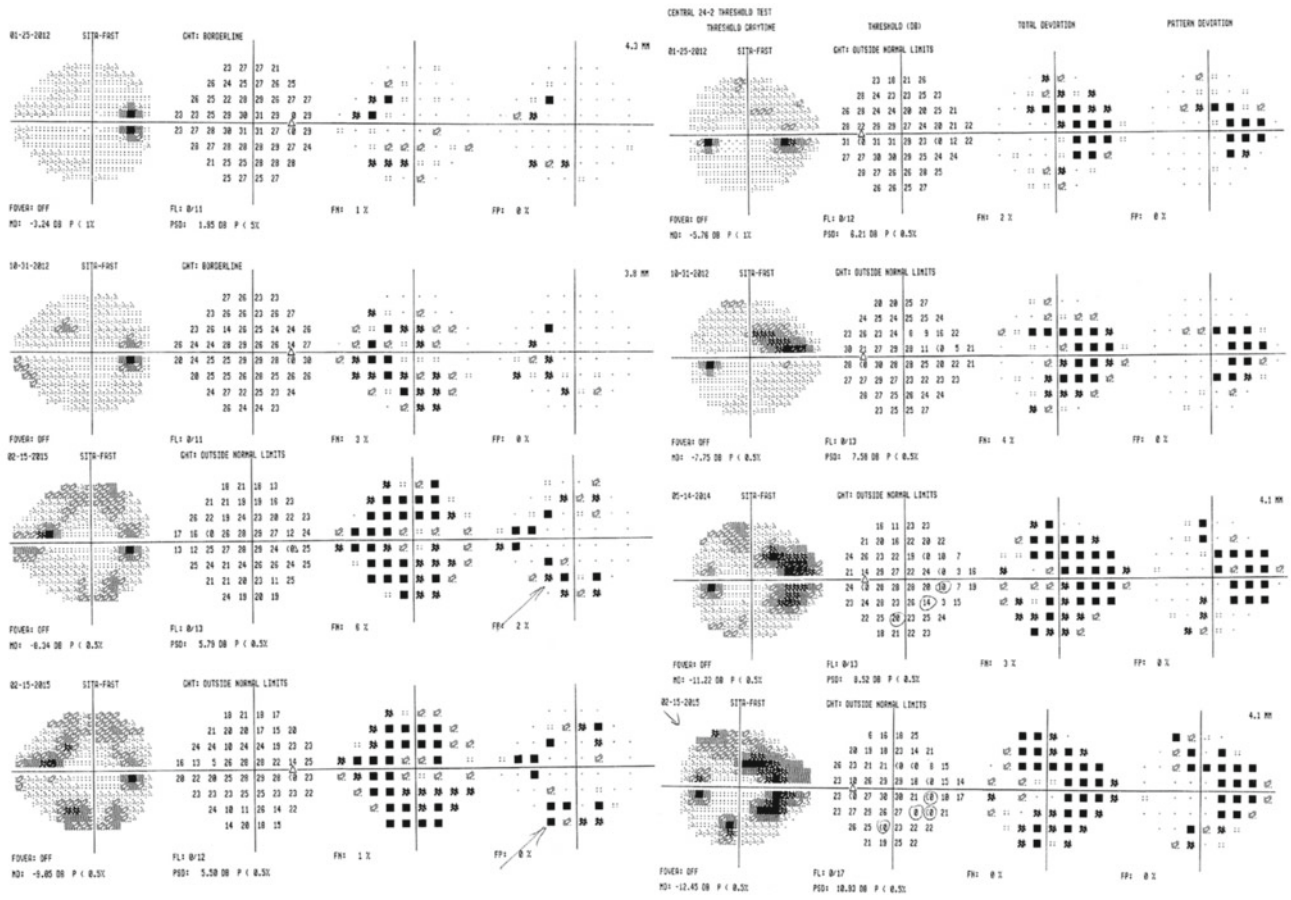
Fig. 10.33 Serial visual field examinations (the same patient in Fig. 10.32) reveal progressive visual field loss over 3 years, despite a normal intraocular pressure. Visual field deficit is compatible with areas of involvement in the fundus autofluorescence and fluorescein angiography images
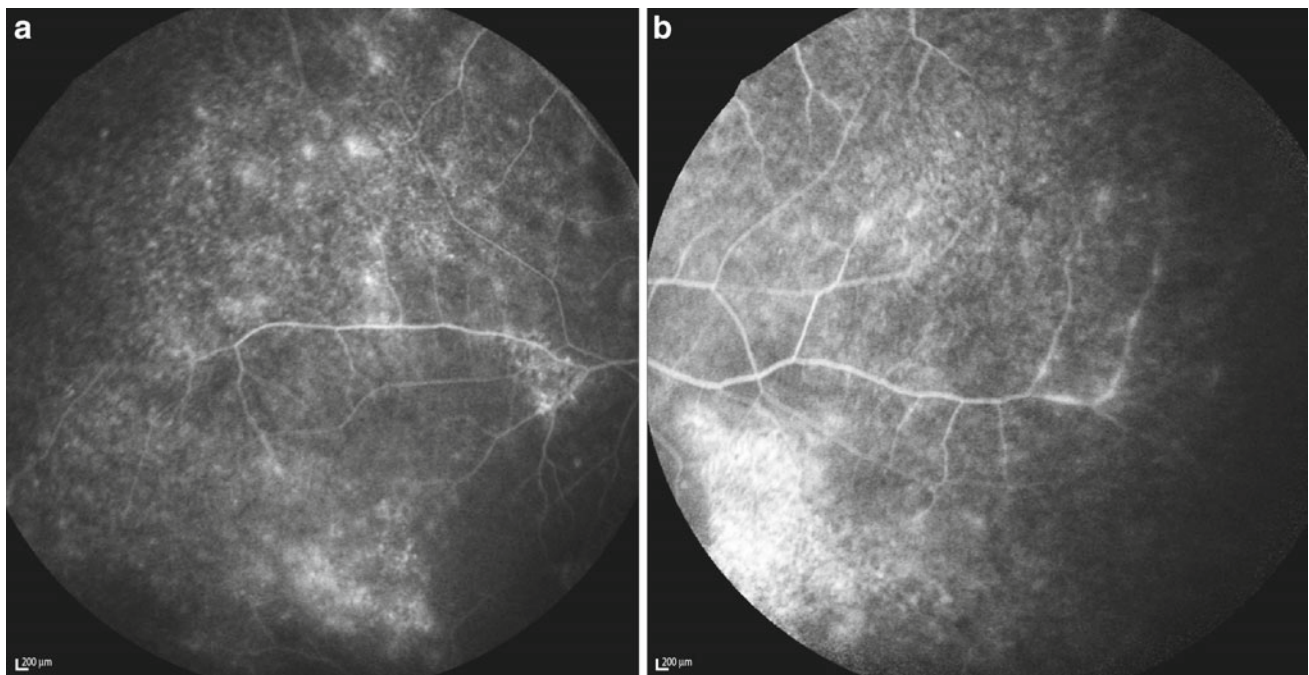

Fig. 10.34 Fluorescein angiography of **a** the right eye (the same patient in Fig. 10.32) and **b** the left eye illustrates peripheral perivascular leakage with diffuse vascular wall staining (i.e., phlebitis)
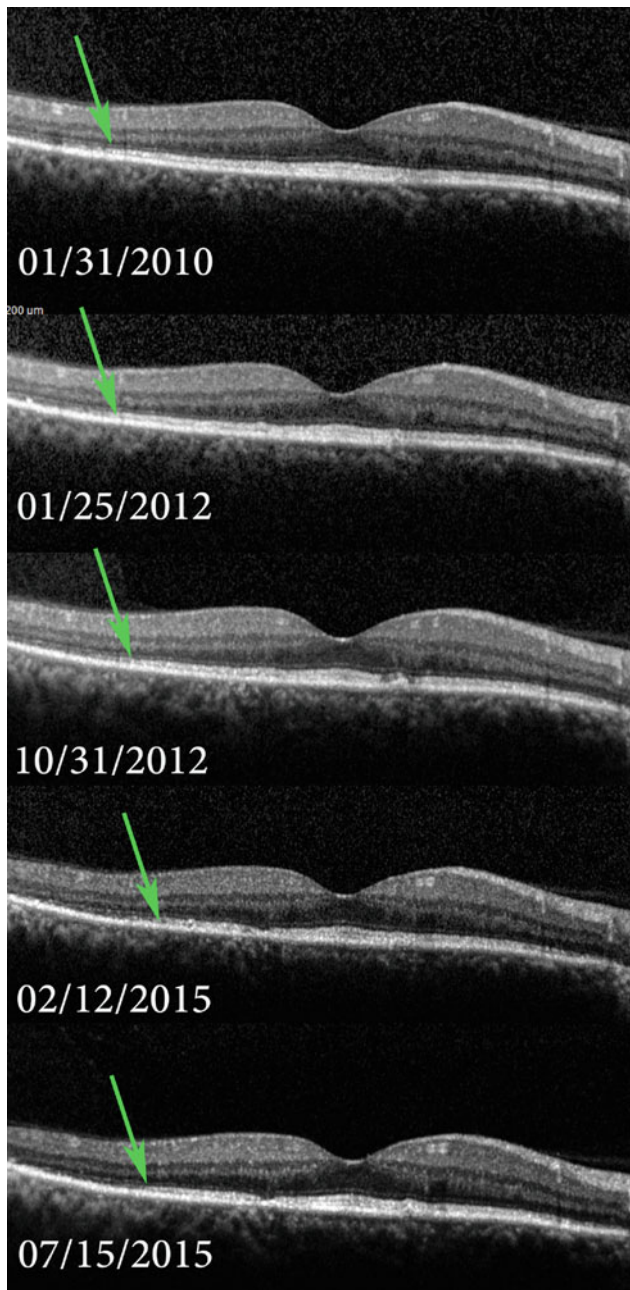
Fig. 10.36 The OCT images of the left eye of the same patient in Fig. 10.32 were obtained a few months apart. The area with normal outer retinal layers has been progressively constricted (*area between the green arrows*). *OCT* optical coherence tomography

Fig. 10.35 Serial OCT images of the right side (the same patient in Fig. 10.32), show progressive loss and attenuation of the external limiting membrane, ellipsoid and interdigitation zone on the temporal side of the macula that correspond to the visual field loss. The cut point of the ellipsoid line is indicated by the green arrows. *IS/OS* inner segment/outer segment, *OCT* optical coherence tomography
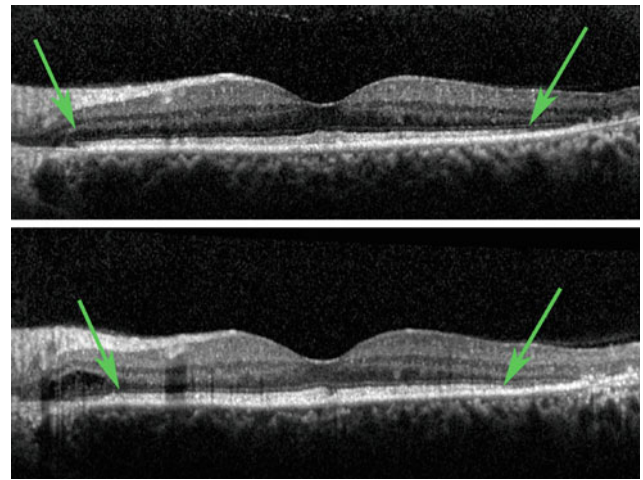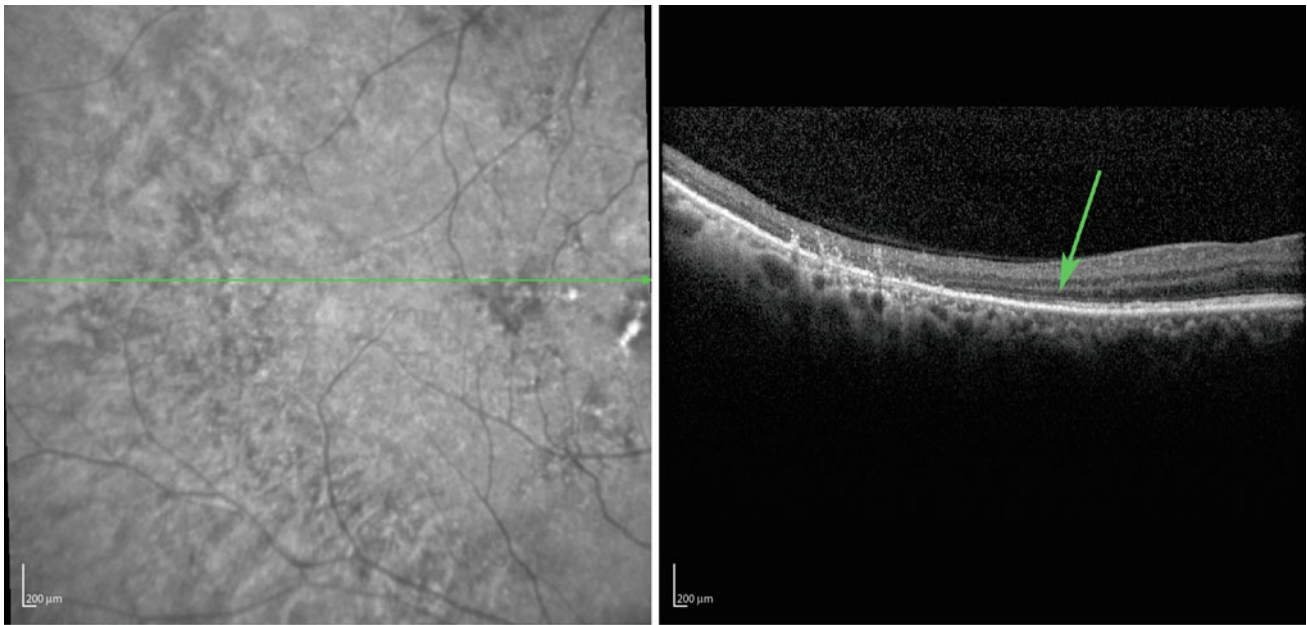
Fig. 10.37 The SLO-OCT image of the temporal right macula (the same patient in Fig. 10.32). Loss of outer retinal layers—comprising the outer nuclear layer, external limiting membrane, ellipsoid zone, and cone outer segment tips—is evident (*green arrow shows the border of* *the abnormal retina in the temporal and normal retina in the more nasal part*). SLO-OCT scanning laser ophthalmoscopy optical coherence tomography
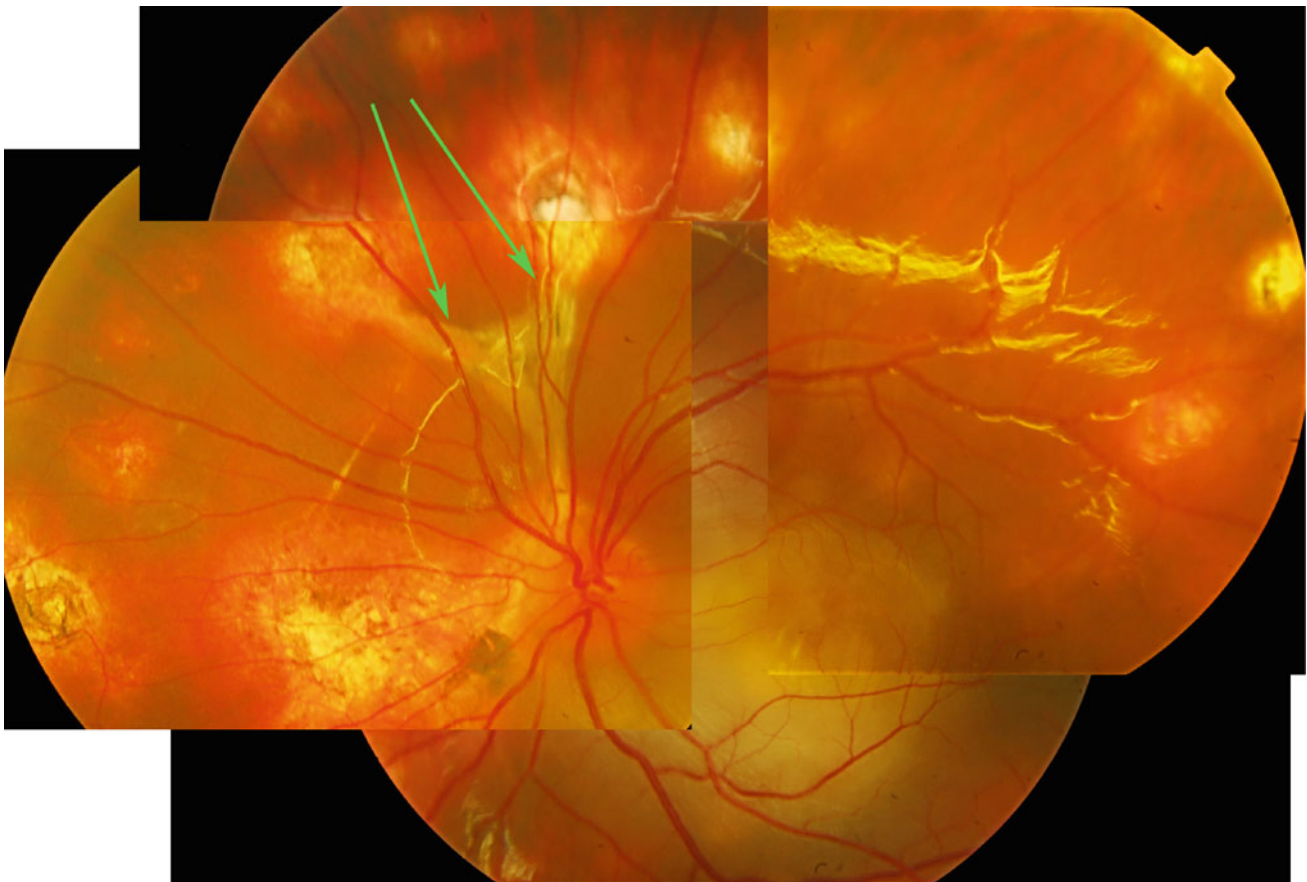

Fig. 10.38 The color fundus photographs from a 15 year-old boy with episodes of decreased vision in the left eye. He had been treated with cytotoxic and steroid agents for years. This image was taken during an episode of deteriorated vision and recurrence of disease. Extensive subretinal fibrosis and posterior pole exudative detachment are visible. The linear streak in the equator, which is parallel to the ora serrata, is formed by the progression and fusion of punched out lesions (Schlaegel line, *arrows*). These lesions are in the RPE and Bruch's membrane and sometimes involve the choriocapillaris layer. *RPE* retinal pigment epithelium
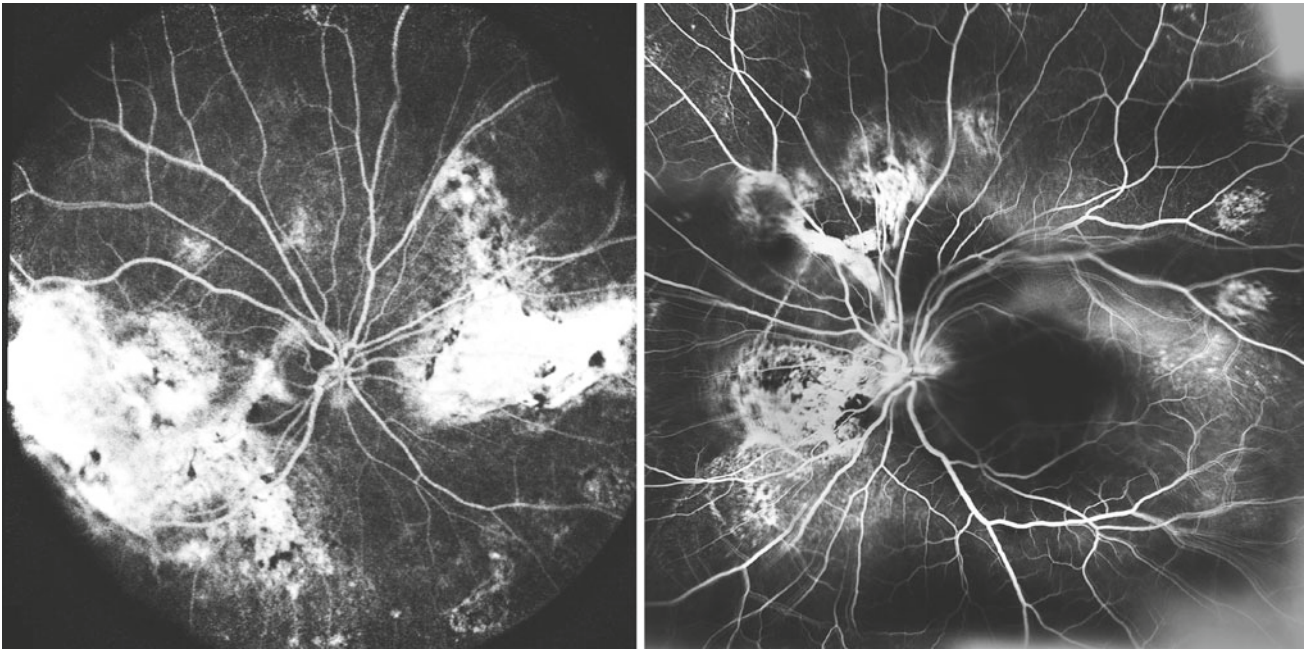
Fig. 10.39 Fluorescein angiography image of the patient in Fig. 10.38 shows extensive subretinal fibrosis with late phase staining in the peripapillary area of both eyes and the macula of the right eye. Hypofluorescence of the posterior pole in the left side results from subretinal exudate accumulation and exudative detachment
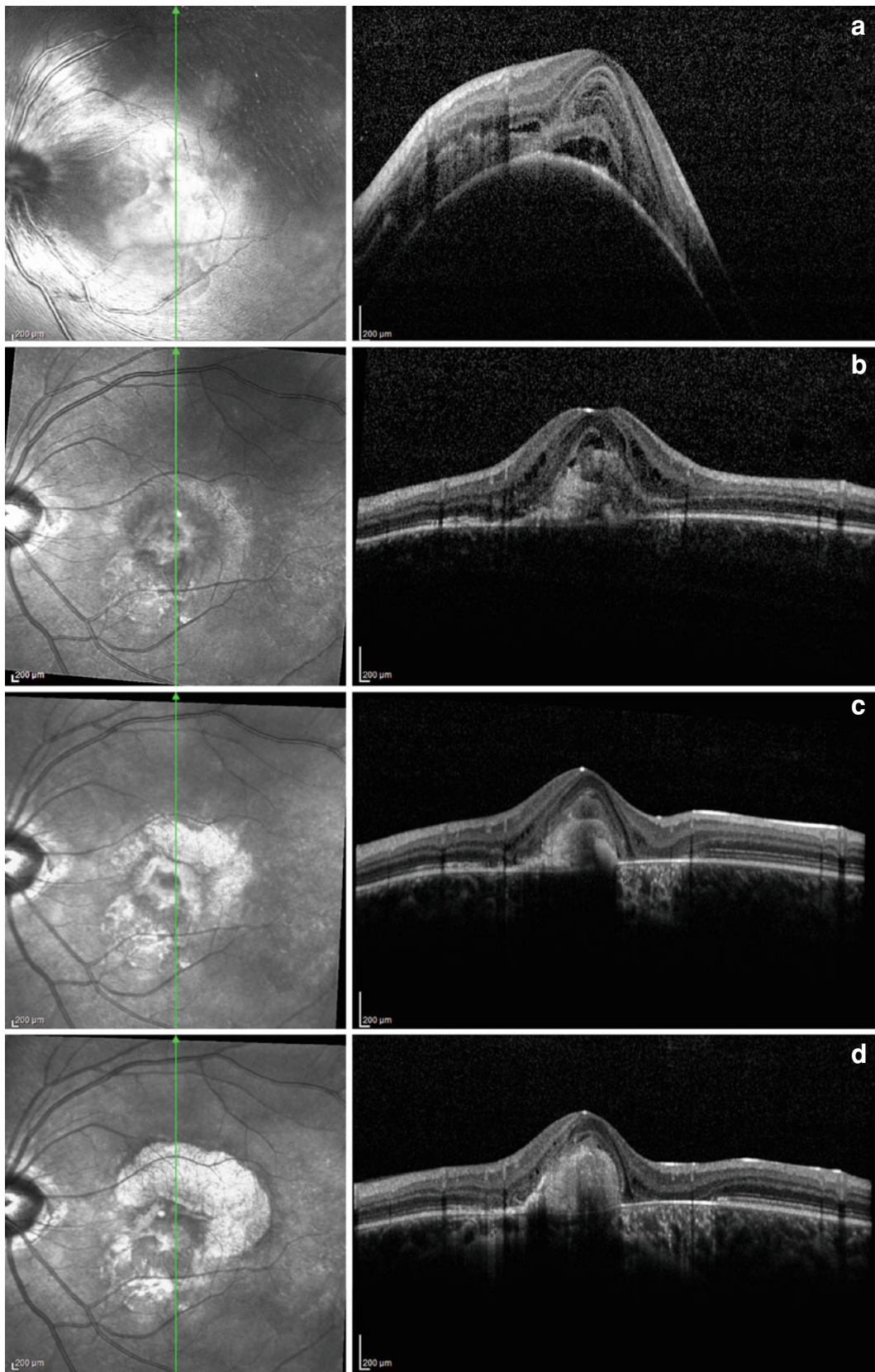
Fig. 10.40 Serial SLO-OCT images of the left eye of the same patient in Fig. 10.38. **a** Exudative detachment with subretinal fibrin deposition, retinal thickening, and disorganization of the photoreceptor layer are evident. **b** Three years after starting treatment, he developed another episode of decreased vision. Neovascular membrane growth along with foveal structure disorganization had occurred. **c** At 1 year after treatment with intravitreal anti-VEGF injection, the findings are scar tissue and fibrosis formation with an area of RPE defects. **d** Regrowth of neovascular tissue with further damage and atrophy of the RPE layer have occurred. *RPE* retinal pigment epithelium, *SLO-OCT* scanning laser ophthalmoscopy optical coherence tomography, *VEGF* vascular epithelium growth factor
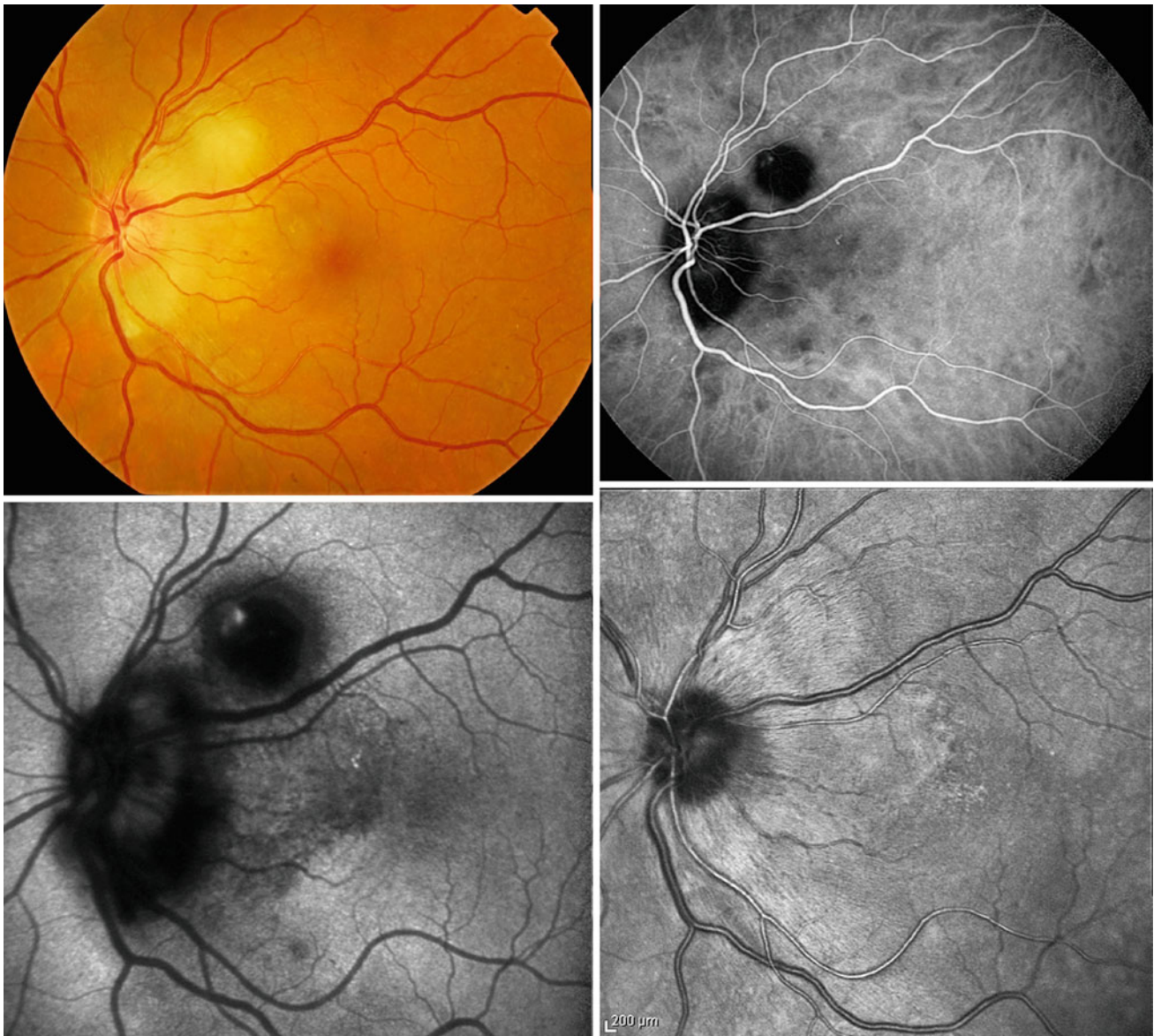
Fig. 10.41 The color fundus photograph and ICG angiography, FAF, and SLO images of a 56 year-old woman with decreased vision in the left eye (20/60). She had a positive quantiferon and PPD test in the absence of pulmonary tuberculosis. Multiple yellow/white peripapillary deep lesions are visible in the color fundus photograph, and represent choroid tubercles. Corresponding to these lesions are hypocyanescent areas in the early phase of ICG angiography (*upper right image*) and hypoautofluorescent round areas in FAF image (*lower left*), which are not detectable in the SLO image (*lower right*). *FAF* fundus autofluorescence, *ICG* indocyanine green, *PPD* purified protein derivative, *SLO* scanning laser ophthalmoscopy
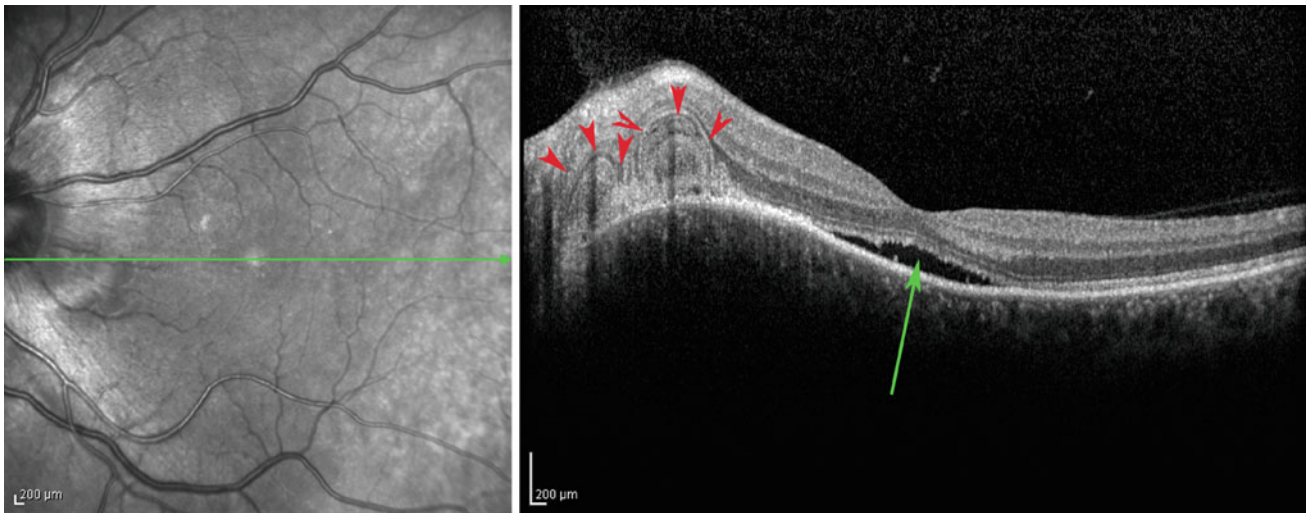
Fig. 10.42 The SLO-OCT scan crosses the central fovea and shows subfoveal serous detachment of the retina (*green arrow*). In the peripapillary area, outer retinal disintegration and exudate accumulation over a choroidal granuloma (*red arrowheads*) are remarkable. Choroidal infiltration and edema resulted in a choroidal bulge in that area. *SLO-OCT* scanning laser ophthalmoscopy optical coherence tomography
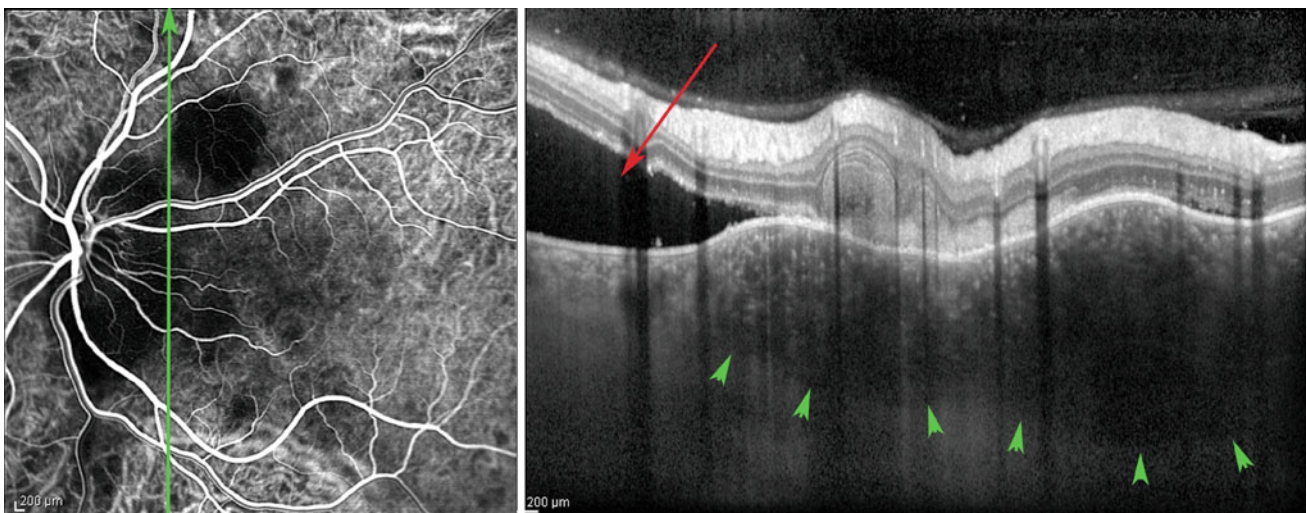
Fig. 10.43 The ICG-EDI-OCT images pass through the largest granulomas in the peripapillary area. A considerable amount of serous fluid is in the inferior part (*red arrow*). Two large hyporeflective choroidal granulomas, which raised the RPE-choriocapillaris complex, are delineated on the EDI image (*green arrowheads*). An exudate with outer retinal disorganization over the granulomas is visible. EDI enhanced depth imaging, ICG indocyanine green, *OCT* optical coherence tomography

Fig. 10.44 Color fundus photographs obtained **a** before treatment and **b** 1 month after treatment with antituberculosis agents and corticosteroid treatment. **c** The EDI-OCT scan crosses the active granulomatous lesion of the choroid before treatment. **d** The EDI-OCT image at the same location after treatment. The green arrowheads outline the outer border of the choroid. Resolution of serous detachment is also notable. *EDI* enhanced depth imaging, *OCT* optical coherence tomography

Fig. 10.45 The SLO-OCT images were obtained **a** before treatment and **b** after treatment. Resolution of the subretinal exudate (*green arrows*) and restoration of the IS/OS junction (*green arrowheads*) are remarkable. *IS/OS* inner segment/outer segment, *SLO-OCT* scanning laser ophthalmoscopy optical coherence tomography
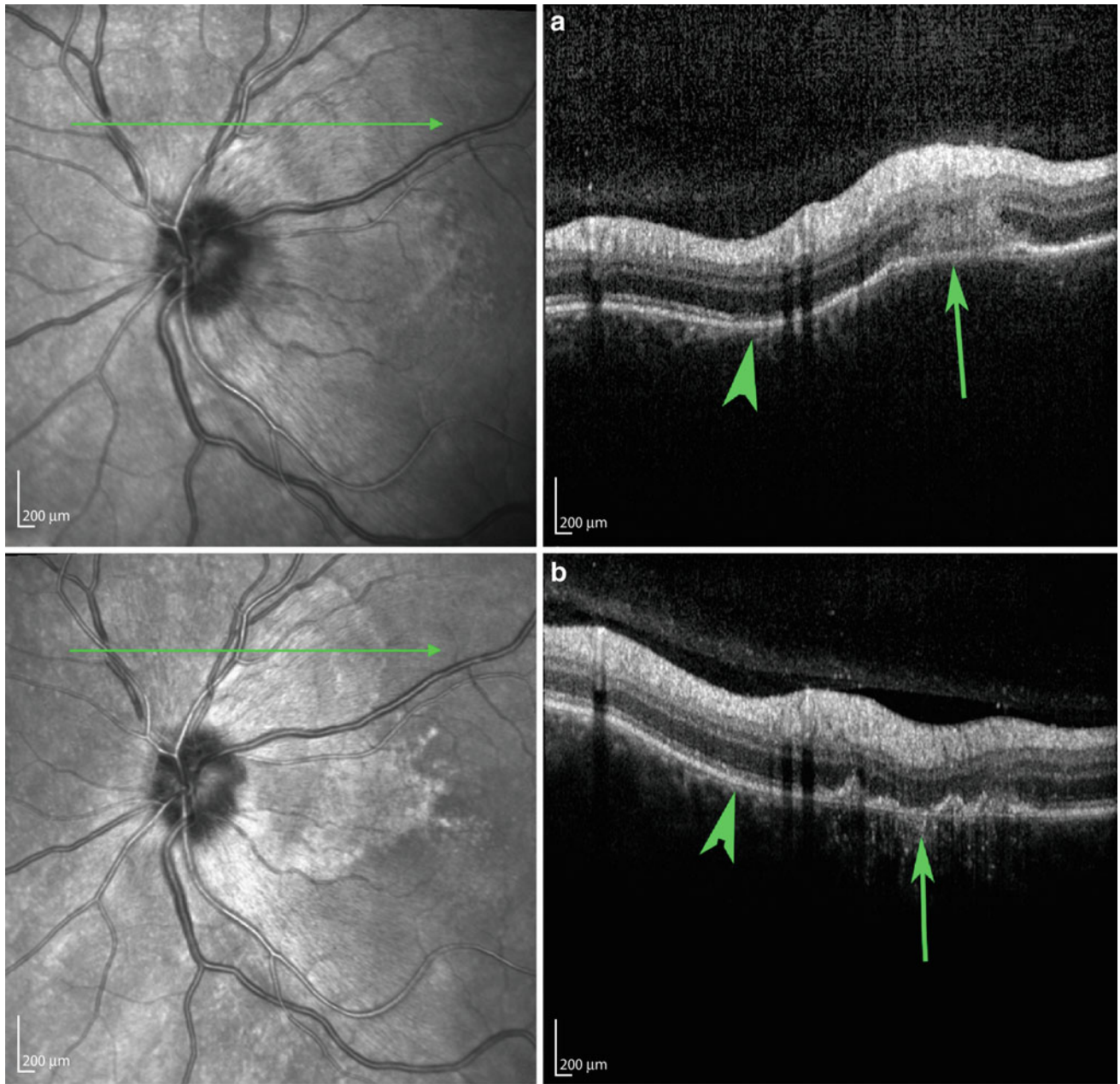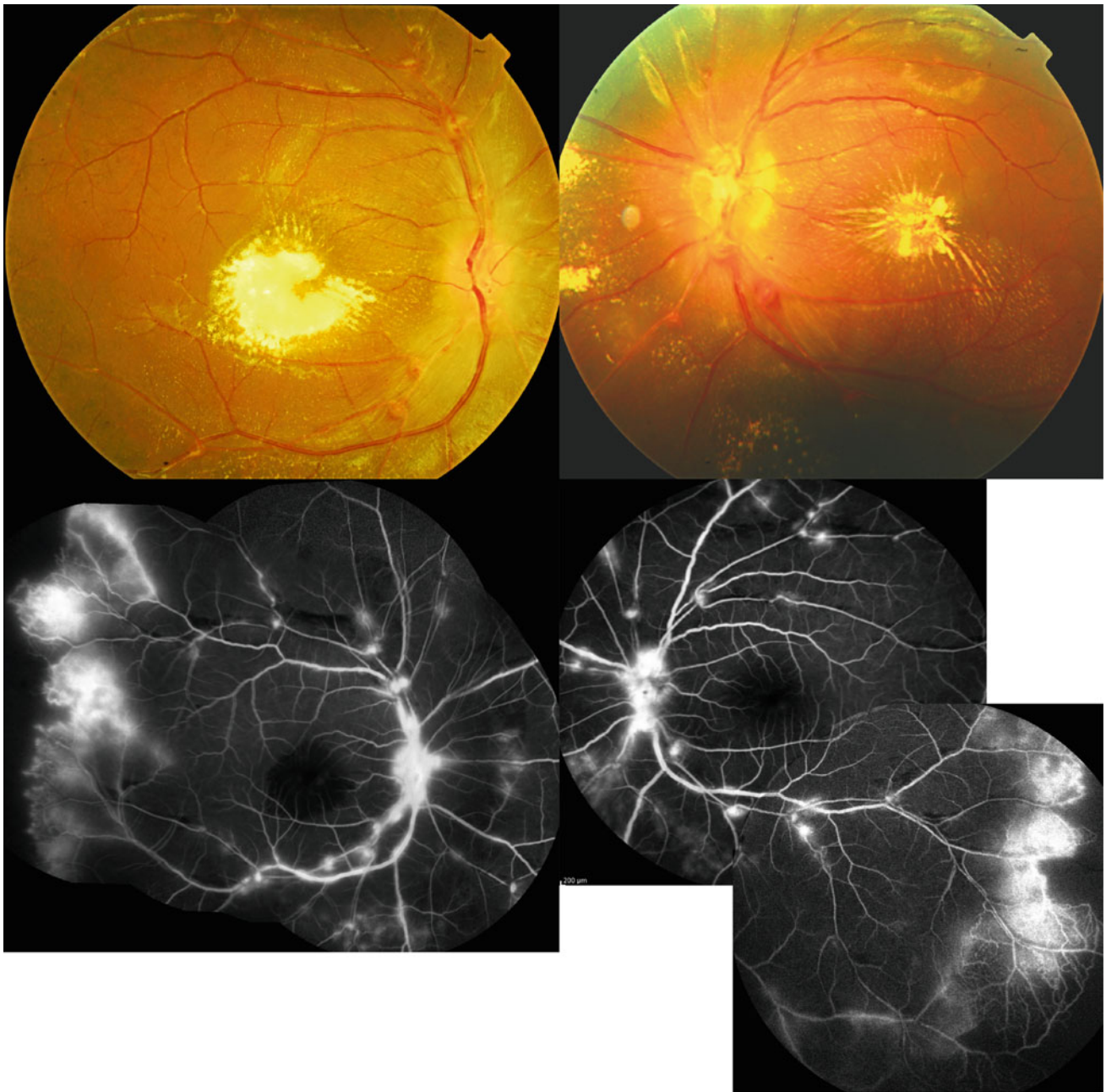
Fig. 10.46 Color fundus photographs from a 13 year old boy with severe decreased vision in both eyes, especially the right eye. Severe papillitis with hard exudate deposits at the foveal area are visible in the fundus photographs. In fluorescein angiography, macroaneurysms are clustered on both optic discs and arterial bifurcations are associated with leakage. Other prominent features in fluorescein angiography are diffuse peripheral retinal vasculitis and capillary nonperfusion

Fig. 10.47 **a** The SLO-OCT image of the right eye (the same patient in Fig. 10.46) at the patient's first visit. Subfoveal hard exudate deposition appears as hyperreflective material in the OCT im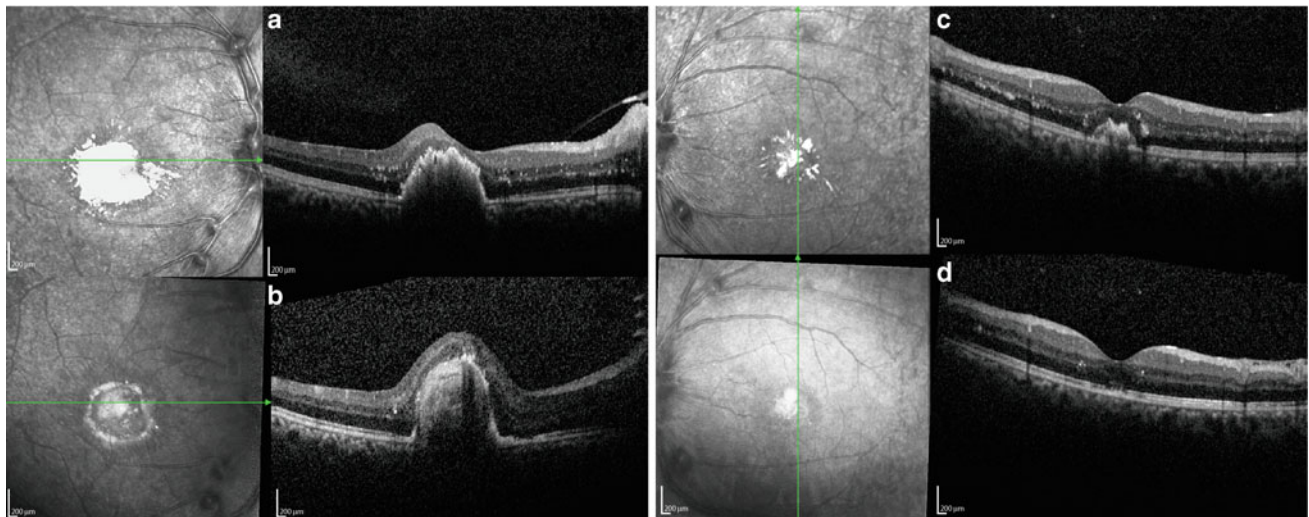age. Foveal photoreceptor disruption is notable, which predicts poor visual outcome. Macular edema is not significant. **b** The SLO-OCT image of the right eye, obtained 5 months after treatment with panretinal photocoagulation and anti-VEGF therapy, shows a persistent subfoveal hyperreflective lesion (i.e., exudate) with partial attenuation of the deposits. **c** The SLO-OCT image of the left eye at the first visit. There are fewer hard exudate deposits, compared to the right macula, and no macular edema. **d** The SLO-OCT image of the left eye, obtained 5 months posttreatment, shows remarkable resorption of the hard exudate, decreased thickening, and partial restoration of foveal photoreceptor arrangement; these phenomena were accompanied by visual gain. *SLO-OCT* scanning laser ophthalmoscopy optical coherence tomography, *VEGF* vascular endothelial growth factor
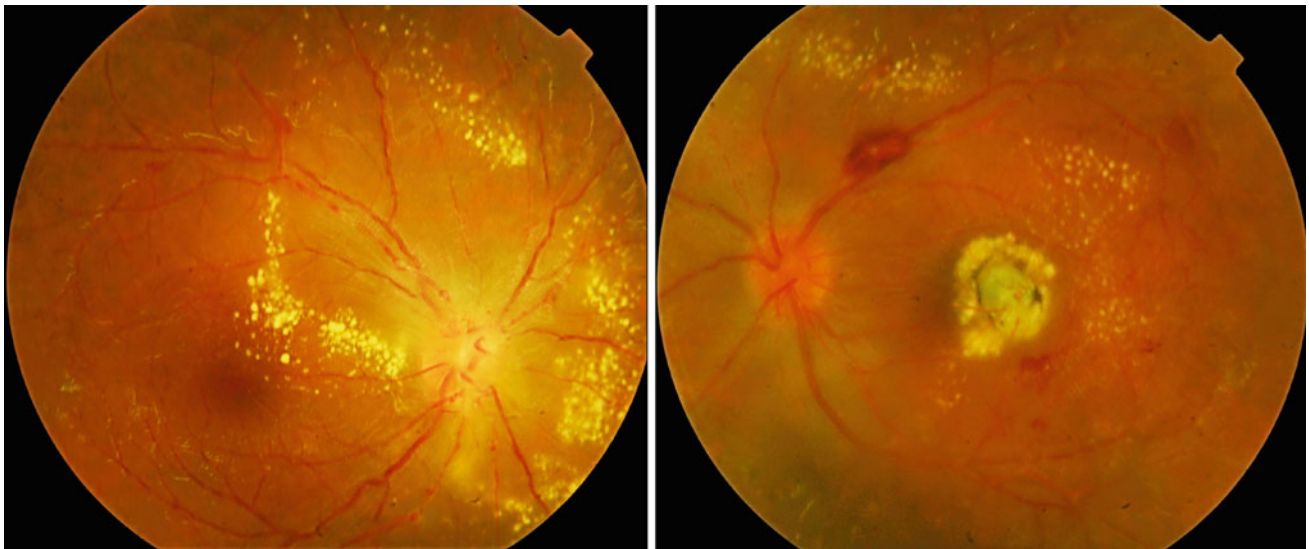
Fig. 10.48 Color fundus photographs of a 23 year-old woman with a 1 year history of decreased vision in the left eye. In examination, visual acuity of the right eye was 20/30 and the left eye was less than 20/200. Deposition of hard exudates in the peripapillary area of the right eye and macula of both eyes, which involved the central fovea in the left eye, is evident in the fundus photographs. In addition, preretinal hemorrhage and scar and pigmentation of the central foveal are remarkable in the left eye
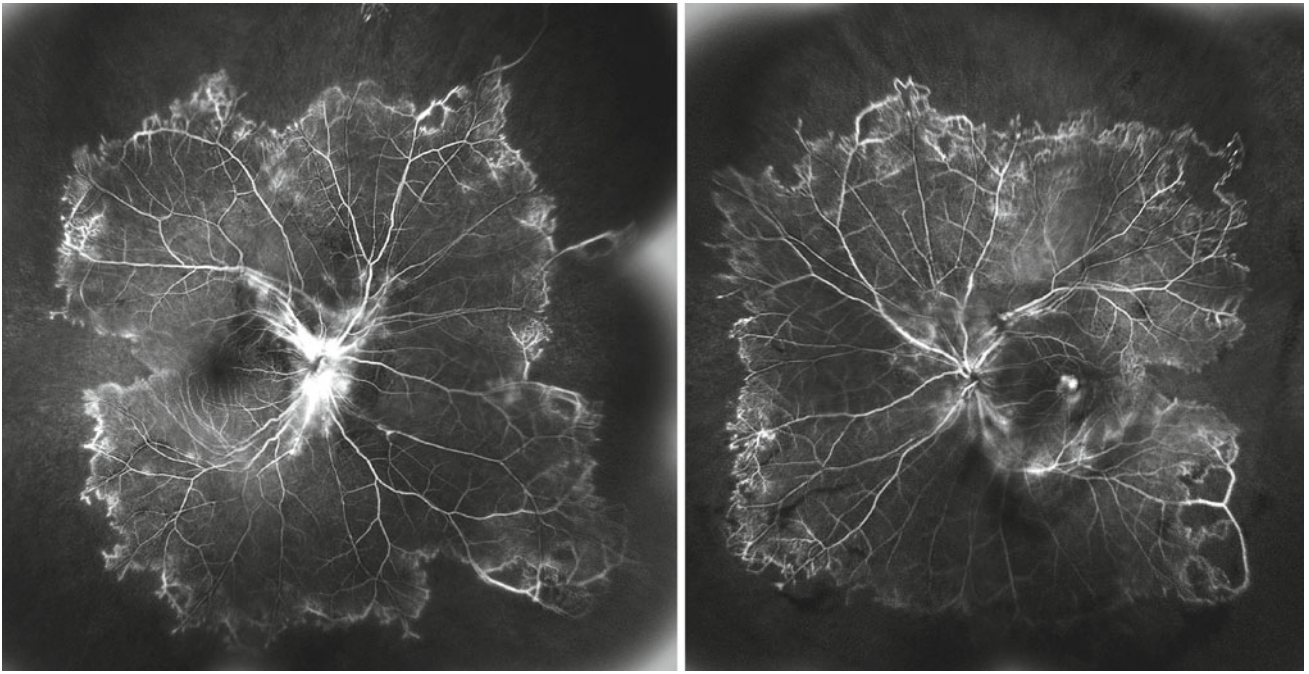
Fig. 10.49 The fluorescein angiography images of both eyes of the same patient in Fig. 10.48 show diffuse peripheral ischemia and capillary nonperfusion areas. Late optic disc leakage and vasculitis are evident
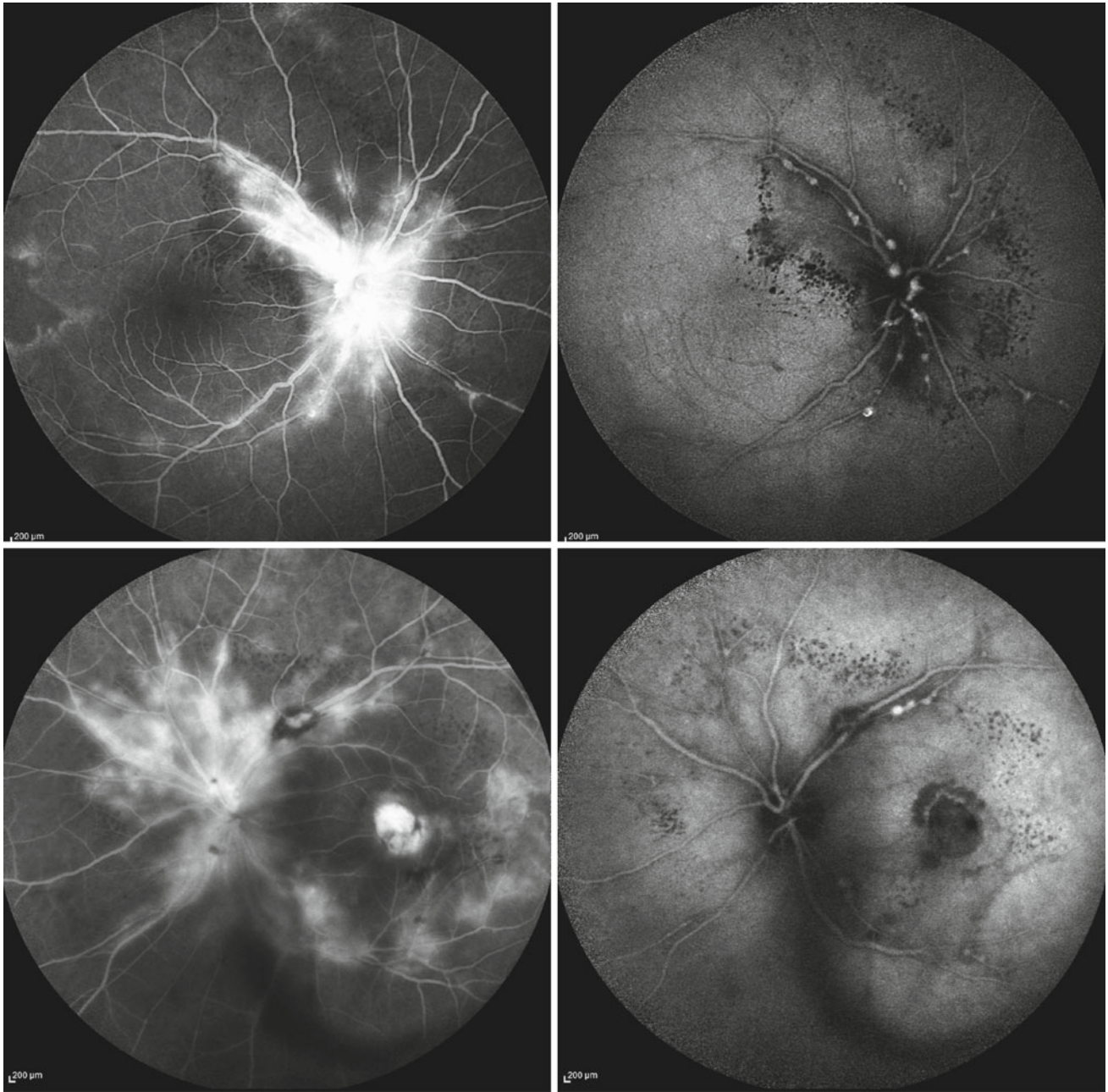
Fig. 10.50 Fluorescein angiography (recirculation phase) and indocyanine green angiography (late phase) of the same patient in Figs. 10.48 and 10.49. Considerable leakage of optic disc and large peripapillary vessels are notable in both eyes in fluorescein angiography. Staining or severe leakage in left fovea is also notable. Late phase indocyanine green angiography of both eyes highlight tied-knot aneurysms because of the lack of dye leakage. They appear as vascular beading and localized saccular dilation of large vessels, which remained filled and stained until the late stages
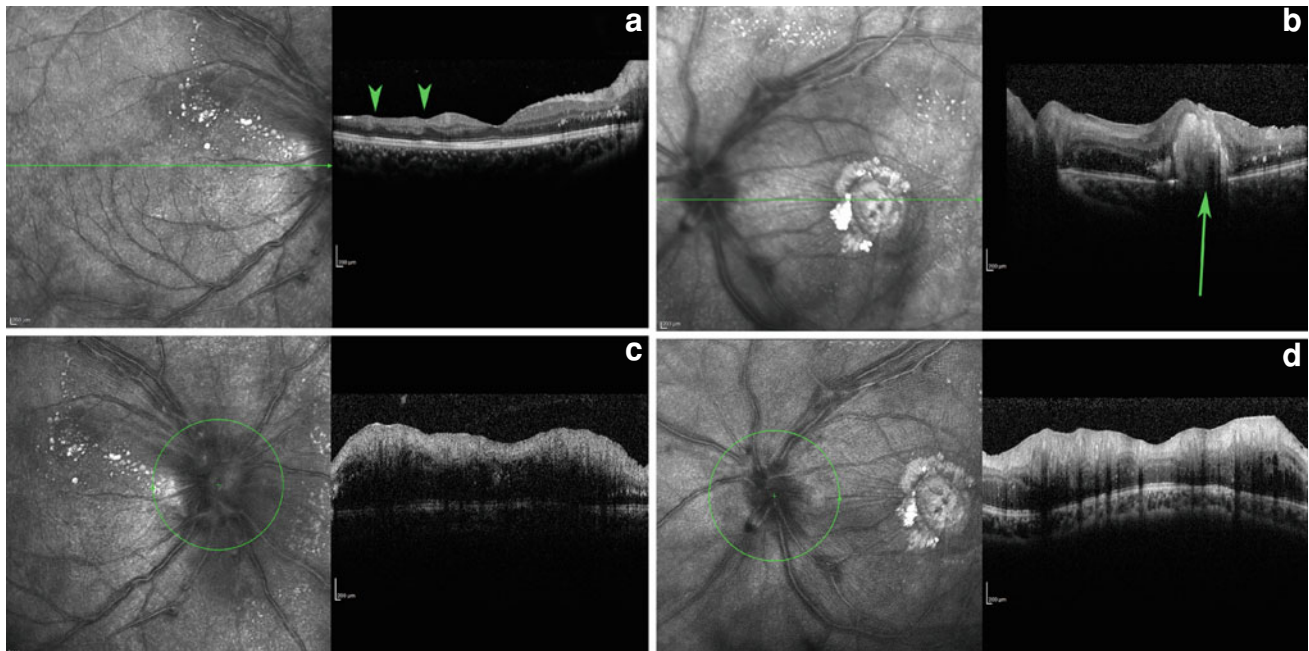
Fig. 10.51 The SLO-OCT images of both eyes of the same patient in Fig. 10.48. **a** Retinal edema in peripapillary area with temporal macular atrophy secondary to small microvasculopathies and occlusive vasculitis that mostly involve the inner part of the retina (*green arrowheads*) are notable. **b** Generalized macular thickening, especially of the nerve fiber layer, is evident. Subfoveal hyperreflectivity in OCT images represents dense subfoveal hard exudate deposition that disrupted the foveal photoreceptors (*green arrow*). **c** and **d** Peripapillary nerve fiber layer thickening is remarkable. OCT optical coherence tomography, SLO scanning laser ophthalmoscopy

10.14 APMPPE

Acute posterior multifocal placoid pigment epitheliopathy (APMPPE) is an idiopathic inflammatory posterior uveitis which is characterized by yellow-white placoid lesion. These plaques are better highlighted using ICGA which illustrates hypocyanescence throughout the study, indicating ischemia of the choriocapillaris as the underlying cause. OCTA showed that even with recovery of the lesions, the choriocapillaris layer nonperfusion does not resolve completely.

OCT depicts disruption of EZ and IZ accompanied by hyper-reflectivity along the outer retinal layers. ELM is also disrupted in most cases [55]. RPE may show hypertransmission or areas of proliferation as well. These areas of initial RPE proliferation later evolves into clinical pigment migration visible on fundus examination. During the course of the disease, complete or incomplete restoration of the respective layers may ensue. The outcome is usually favorable; however, attenuation of outer retinal layers and RPE irregularities may remain [56] (Figs. 10.52, 10.53 and 10.54).
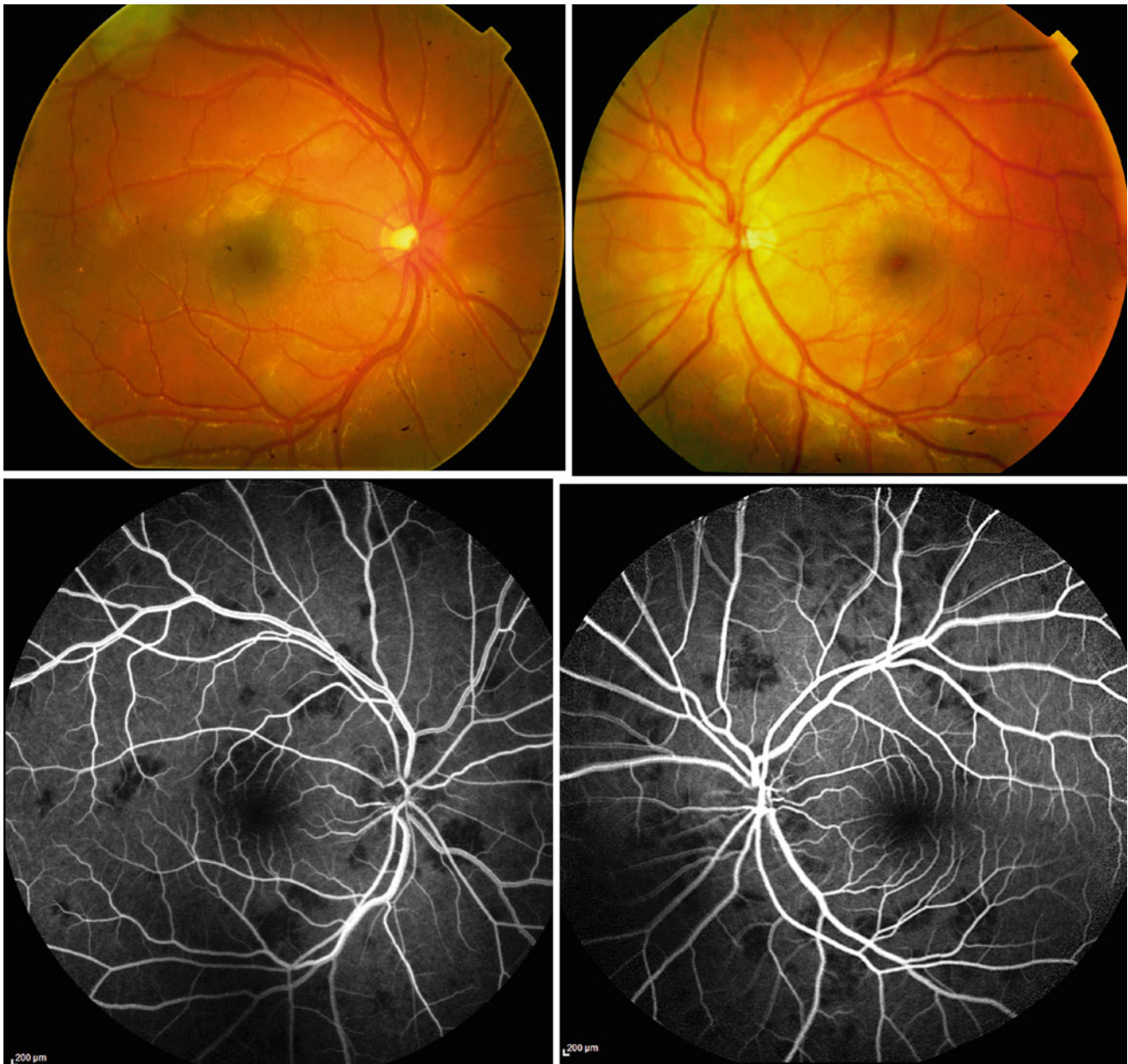
Fig. 10.52 Fundus photo and fluorescein angiography (FA) of a patient with the diagnosis of Acute posterior multifocal placoid pigment epitheliopathy (APMPPE): upper row: fundus photo shows deep multifocal placoid yellow lesions in both eyes. Lower row: FA clearly shows hypofluorescent patches
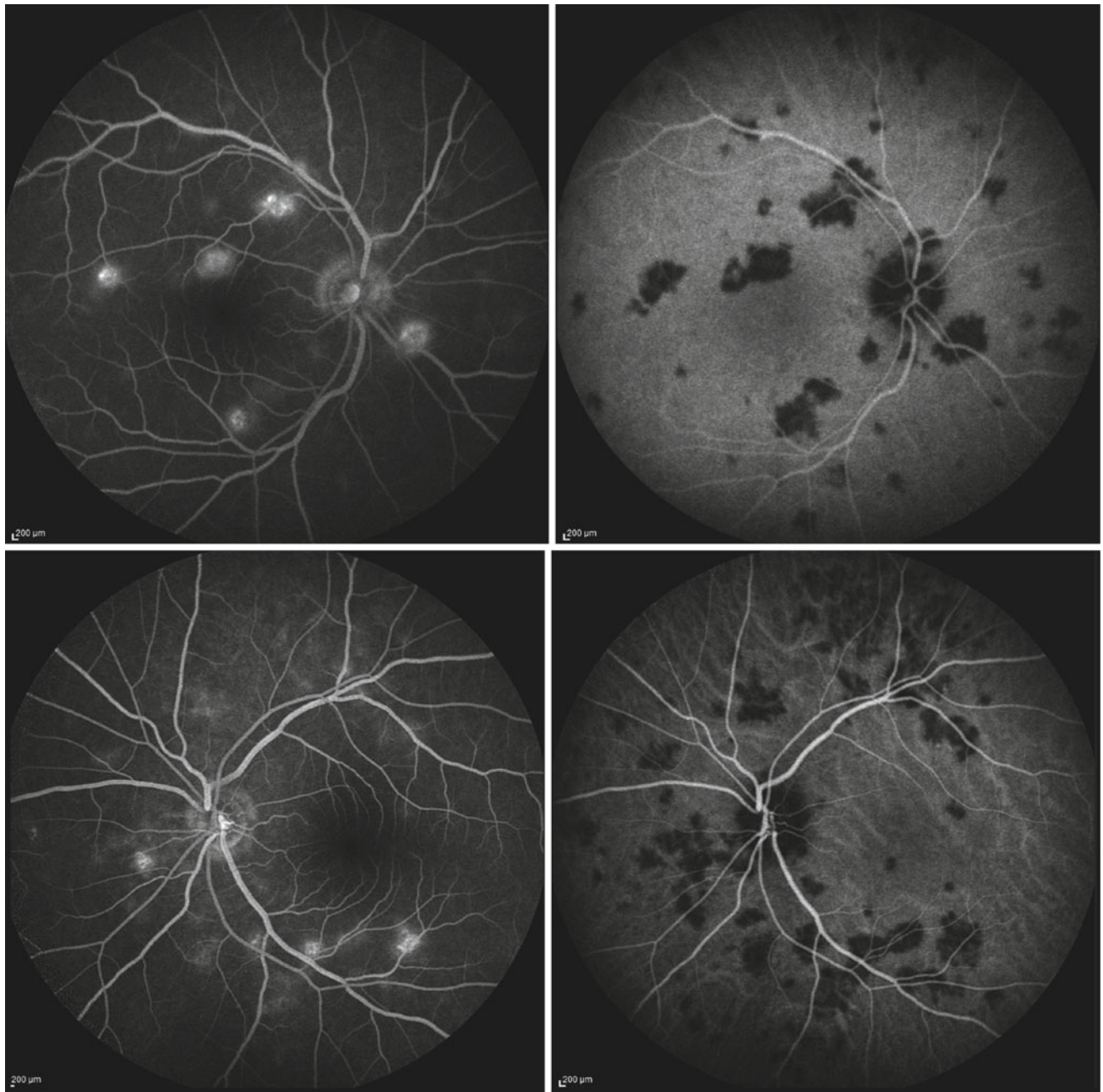
Fig. 10.53 Shows fluorescein angiography (FA) and indocyanine green angiography of the patient with AMPEE in Fig. 10.52: Left column: late phases of FA in both eyes show staining and leakage of the lesions however in ICGA in the right column hypocyanescence is preserved from early to late phases of the angiogram
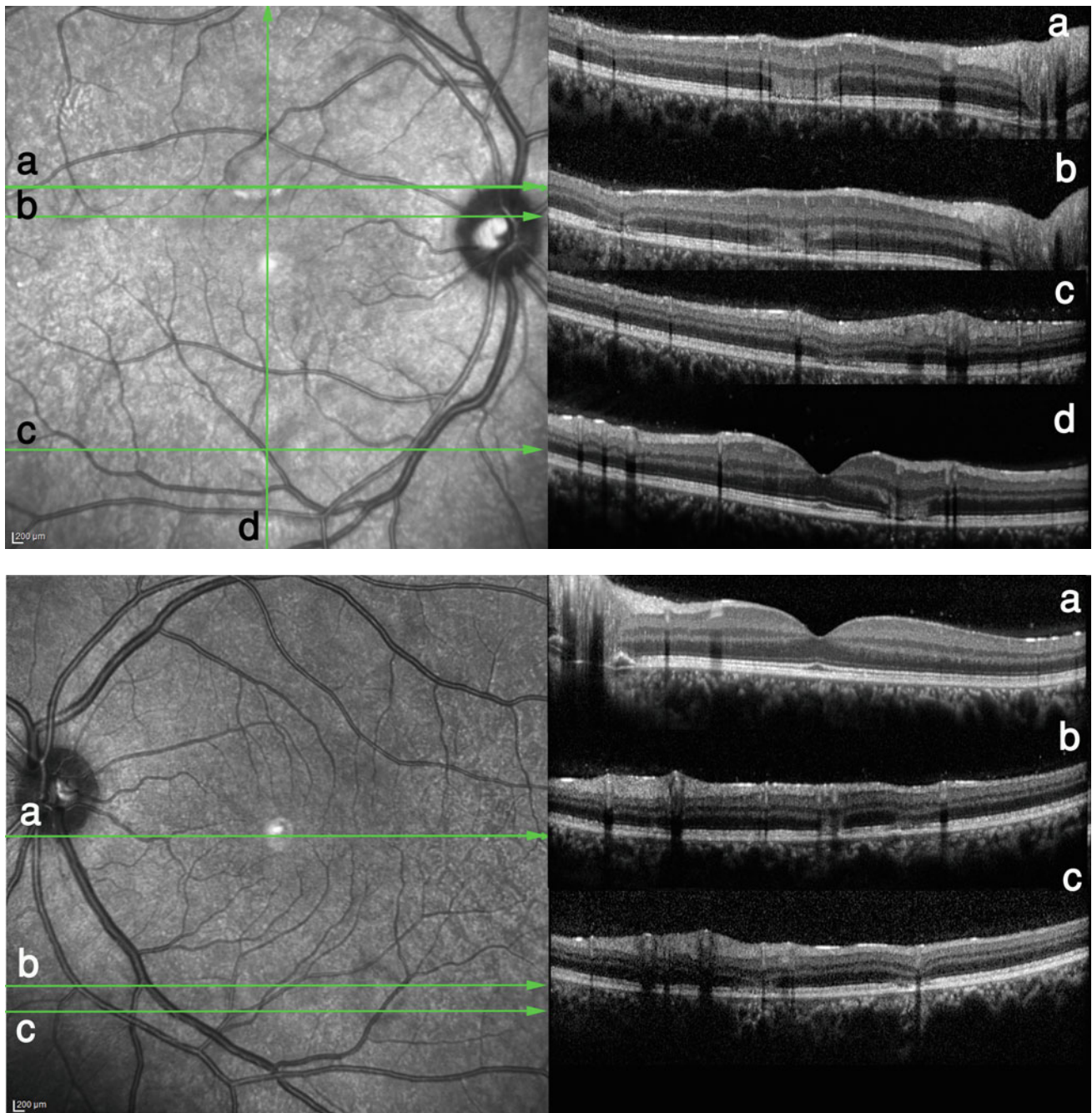
Fig. 10.54 OCT scans of both eyes of the patient with APMPPE in Fig. 10.52: In areas of active lesions, the inflammation of the choriocapillaris manifest with outer retina hyperreflectivity. Please note that the central fovea of both eyes are well-preserved. Also in areas of active lesion, hyporeflectivity of choriocapillaris is evident which is more clearly seen in EDI-OCT images

Fig. 10.55 The FAF-SLO-FA images of right eye of an 11 year-old boy with a chief complaint of decreased vision in the right eye. His history is positive for varicella infection (i.e., small pox) 10 days before presentation. Cilioretinal artery occlusion is evident in these photos. The FAF image reveals an area of hypoautofluorescence, which is distributed around the cilioretinal artery, and results from severe edema and fluid retention that obscure the underlying RPE. In the SLO image, hyporeflectivity of the involved area is a characteristic finding in retinal artery occlusion. The FA image, obtained 34 s after the dye injection, reveals a delay in cilioretinal artery filling. *FA* fluorescein angiography, *FAF* fundus autofluorescence, *RPE* retinal pigment epithelium, *SLO* scanning laser ophthalmoscopy
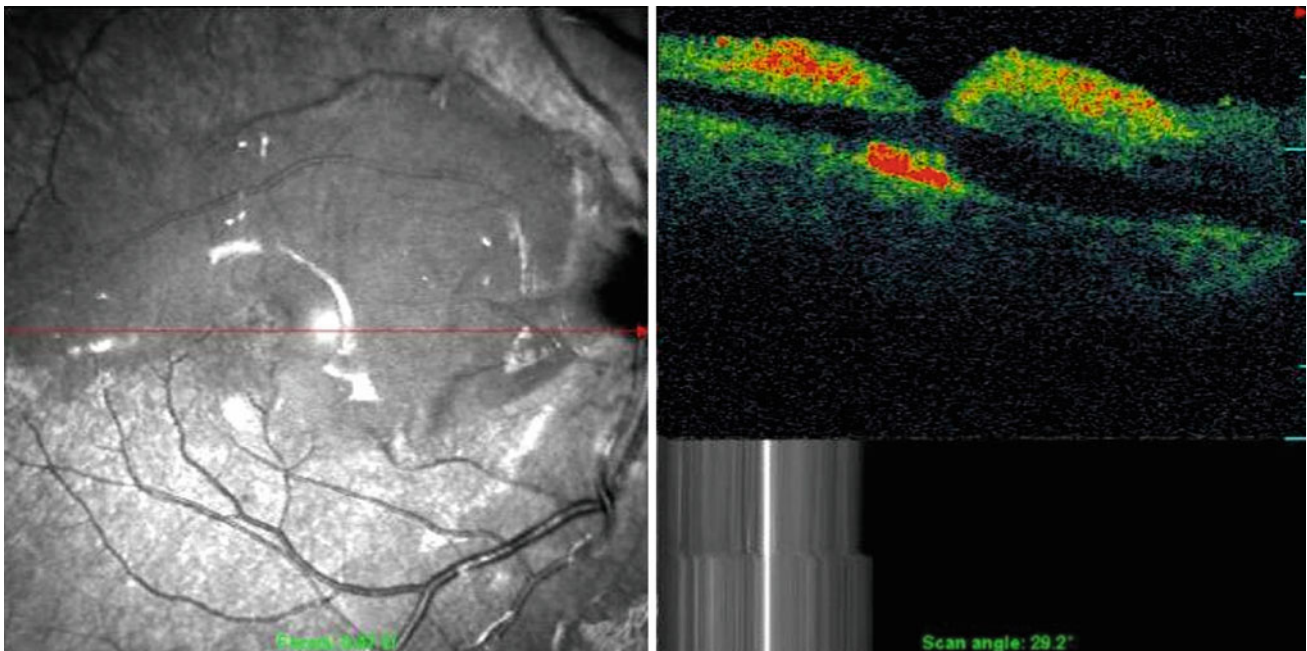
Fig. 10.56 In the SLO-OCT image, (the same patient in Fig. 10.55) signs of inner retinal edema and high reflectivity and retinal thickening are notable. Thickening and high inner reflectivity is absent in the central fovea because of the absence of the inner layer in the foveola. This is a characteristic OCT finding in BRAO involving the fovea. *BRAO*, branch retinal artery occlusion, *OCT* optical coherence tomography, *SLO* scanning laser ophthalmoscopy

10.15 Miscellaneous

Viral infections, especially the herpes family of viruses (e.g., cytomegalovirus, herpes simplex virus, herpes zoster virus), can involve the retina and result in retinal vasculitis and retinitis [57]. Necrotizing retinitis regardless of the etiology appears as hyper-reflective disruption of the normal architecture of the retina [58]. CMV can invade the eye through choroidal or retinal vasculature and can cause necrotizing retinitis in immunocompromised individuals. It infects RPE, Muller cells and inner retinal layers, with relative sparing of the photoreceptors [59]. Involvement of Muller cells may appear as vertical line connecting RPE to inner retinal layers, sparing the outer photoreceptors [60]. OCT can demonstrate two patterns for CMV retinitis: (1) full thickness pattern: hyper-reflectivity and disruption of the retinal architecture. (2) Cavernous pattern: distorted architecture of ONL by cystoid spaces or largely optically empty spaces results in appearance of a single hyper-reflective structure.

There is one report of branch arteriolar occlusion associated with chicken-pox in the literature [61], similar to the finding in the patient presented in Figs. 10.55 and 10.56.

References

1. Lardenoye CW, van Kooij B, Rothova A. Impact of macular edema on visual acuity in uveitis. Ophthalmol. 2006;113:1446–9.
2. Gallagher MJ, Yilmaz T, Cervantes-Castañeda RA, Foster CS. The characteristic features of optical coherence tomography in posterior uveitis. Br J Ophthalmol. 2007;91:1680–5.
3. Munk MR, Sacu S, Huf W, et al. Differential diagnosis of macular edema of different pathophysiologic origins by spectral domain optical coherence tomography. Retina. 2014;2014(34):2218–32.
4. Saito M, Barbazetto IA, Spaide RF. Intravitreal cellular infiltrate imaged as punctate spots by spectral-domain optical coherence tomography in eyes with posterior segment inflammatory disease. Retina. 2013;33:559–65.
5. Kempen JH, Van Natta ML, Altaweel MM, et al. Multicenter Uveitis Steroid Treatment (MUST) trial research group. Factors predicting visual acuity outcome in intermediate, posterior and panuveitis: the Multicenter Uveitis Steroid Treatment (MUST). Trial Am J Ophthalmol. 2015;160:1133–41.
6. Agarwal A, Invernizzi A, Singh RB et al. An update on inflammatory choroidal neovascularization: epidemiology, multimodal imaging, and management. J Ophthalmic Inflamm Infect. 2018;8:13.
7. Roy R, Saurabh K, Bansal A, et al. Inflammatory choroidal neovascularization in Indian eyes: etiology, clinical features, and outcomes to anti-vascular endothelial growth factor. Indian J Ophthalmol. 2017;65:295–300.
8. Hoang QV, Cunningham Jr ET, Sorenson et al. The "pitchfork sign" a distinctive optical coherence tomography finding in inflammatory choroidal neovascularization. Retina. 2013;33:1049–55.
9. Ebrahimi Z, Torkashvand A, Zarei M, et al. Treatment of inflammatory macular hole: case series and review of literature. Ocul Immunol Inflamm. 2021:1–7.
10. Tugal-Tutkun I. Imaging in the diagnosis and management of Behcet disease. Int Ophthalmol Clin. 2012;52:183–90.
11. Ishikawa S, Taguchi M, Muraoka T, Sakurai Y, Kanda T, Takeuchi M. Changes in subfoveal choroidal thickness associated with uveitis activity in patients with Behçet's disease. Br J Ophthalmol. 2014;98:1508–13.
12. Ataş M, Yuvacı I, Demircan S, Güler E, Altunel O, Pangal E, et al. Evaluation of the macular, peripapillary nerve fiber layer and choroid thickness changes in Behçet's disease with spectral-domain OCT. J Ophthalmol. 2014;2014:865394.
13. Coskun E, Gurler B, Pehlivan Y, Kisacik B, Okumus S, Yayuspayi R, et al. Enhanced depth imaging optical coherence tomography findings in Behcet disease. Ocul Immunol Inflamm. 2013;21:440–5.
14. Lin D, Chen W, Zhang G, Huang H, Zhou Z, Cen L, et al. Comparison of the optical coherence tomographic characters between acute Vogt–Koyanagi–Harada disease and acute central serous chorioretinopathy. BMC Ophthalmol. 2014;14:87.
15. Spaide R. Autofluorescence from the outer retina and subretinal space: hypothesis and review. Retina. 2008;28:5–35.
16. Nicholson B, Noble J, Forooghian F, Meyerle C. Central serous chorioretinopathy: update on pathophysiology and treatment. Surv Ophthalmol. 2013;58:103–26.
17. Yamamoto M, Nishijima K, Nakamura M, Yoshimura N. Inner retinal changes in acute-phase Vogt–Koyanagi–Harada disease measured by enhanced spectral domain optical coherence tomography. Jpn J Ophthalmol. 2011;55:1–6.
18. Nakayama M, Keino H, Okada AA, Watanabe T, Taki W, Inoue M, et al. Enhanced depth imaging optical coherence tomography of the choroid in Vogt–Koyanagi–Harada disease. Retina. 2012;32:2061–9.
19. Takahashi H, Takase H, Ishizuka A, Miyanaga M, Kawaguchi T, Ohno-Matsui K, et al. Choroidal thickness in convalescent Vogt–Koyanagi–Harada disease. Retina. 2014;34:775–80.
20. Hosoda Y, Uji A, Hangai M, Morooka S, Nishijima K, Yoshimura N. Relationship between retinal lesions and inward choroidal bulging in Vogt–Koyanagi–Harada disease. Am J Ophthalmol. 2014;157:1056–63.
21. Tsuboi K, Nakai K, Iwahashi C, Gomi F, Ikuno Y, Nishida K. Analysis of choroidal folds in acute Vogt–Koyanagi–Harada disease using high-penetration optical coherence tomography. Graefes Arch Clin Exp Ophthalmol. 2015;253:959–64.
22. Tanigawa M, Ochiai H, Tsukahara Y, Ochiai Y, Yamanaka H. Choroidal folds in acute-stage Vogt–Koyanagi–Harada disease patients with relatively short axial length. Case Rep Ophthalmol. 2012;3:38–45.
23. Fong AH, Li KK, Wong D. Choroidal evaluation using enhanced depth imaging spectral-domain optical coherence tomography in Vogt–Koyanagi–Harada disease. Retina. 2011;31:502–9.
24. Nazari H, Hariri A, Hu Z, Ouyang Y, Sadda S, Rao NA. Choroidal atrophy and loss of the choriocapillaris layer in convalescent stage of Vogt–Koyanagi–Harada disease: in vivo documentation. J Ophthalmic Inflamm Infect. 2014;4:9. pmid:24655594.
25. Hirukawa K, Keino H, Watanabe T, Okada AA. Enhanced depth imaging optical coherence tomography of the choroid in new-onset acute posterior scleritis. Graefes Arch Clin Exp Ophthalmol. 2013;251:2273–5.
26. Taki W, Keino H, Watanabe T, Okada AA. Enhanced depth imaging optical coherence tomography of the choroid in recurrent unilateral posterior scleritis. Graefes Arch Clin Exp Ophthalmol. 2013;251:1003–4.
27. Oréfice JL, Costa RA, Scott IU, Calucci D, Oréfice F. Grupo Mineiro de Pesquisa em Doenças Oculares Inflamatórias (MINAS). Spectral optical coherence tomography findings in

patients with ocular toxoplasmosis and active satellite lesions (MINAS Report 1). Acta Ophthalmol. 2013;91:e41–7.

28. Laatikainen L, Erkkilä H. Serpiginous choroiditis. Br J Ophthalmol. 1974;58:777–83.

29. Akpek EK, Ilhan-Sarac O. New treatments for serpiginous choroiditis. Curr Opin Ophthalmol. 2003;14:128–31.

30. Hamilton AM, Bird AC. Geographical choroidopathy. Br J Ophthalmol. 1974;58:784–97.

31. Abrez H, Biswas J, Sudharshan S. Clinical profile, treatment, and visual outcome of serpiginous choroiditis. Ocul Immunol Inflamm. 2007;15:325–35.

32. De Bats F, Wolff B, Vasseur V, Affortit A, Kodjikian L, Sahel JA, et al. "En-face" spectral-domain optical coherence tomography findings in multiple evanescent white dot syndrome. J Ophthalmol. 2014;2014:928028.

33. Pakzad-Vaezi K, Or C, Yeh S, Forooghian F. Optical coherence tomography in the diagnosis and management of uveitis. Can J Ophthalmol. 2014;49:18–29.

34. Mrejen S, Khan S, Gallego-Pinazo R, Jampol LM, Yannuzi LA. Acute zonal occult outer retinopathy: a classification based on multimodal imaging. JAMA Ophthalmol. 2014;132:1089–98.

35. Ohta K, Sato A, Fukui E. Spectral domain optical coherence tomographic findings at convalescent stage of acute zonal occult outer retinopathy. Clin Ophthalol. 2009;3:423–8.

36. Makino S, Tampo H. Changes in optical coherence tomography finding in acute zonal occult outer retinopathy. Case Rep Ophthalmol. 2013;4:99–104.

37. Matsui Y, Matsubara H, Ueno S, Ito Y, Terasaki H, Kondo M. Changes in outer retinal microstructures during six month period in eyes with acute zonal occult outer retinopathy-complex. PLoS ONE. 2014;9:e110592.

38. Spaide RF, Goldberg N, Freund KB. Redefining multifocal choroiditis and panuveitis and punctate inner choroidopathy through multimodal imaging. Retina. 2013;33:1315–24.

39. Pirraglia MP, Tortorella P, Abbouda A, Toccaceli F, La Cava M. Spectral domain optical coherence tomography imaging of tubercular chorioretinitis and intraretinal granuloma. Intraretinal tuberculosis: a case report. Int Ophthalmol. 2015;35:445–50.

40. Salman A, Parmar P, Rajamohan M, Vanila CG, Thomas PA, Jesudasan CA. Optical coherence tomography in choroidal tuberculosis. Am J Ophthalmol. 2006;142:170–2.

41. Al-Mezaine HS, Al-Muammar A, Kangave D, Abu El-Asrar AM. Clinical and optical coherence tomographic findings and outcome of treatment in patients with presumed tuberculous uveitis. Int Ophthalmol. 2008;28:413–23.

42. Mehta S. Healing patterns of choroidal tubercles after antitubercular therapy: a photographic and OCT study. J Ophthalmic Inflamm Infect. 2012;2:95–7.

43. Pasadhika A, Rosembaum JT. Ocular Sarcoidosis. Clin Chest Med. 2015;36:669–83.

44. Gass JD, Olson CL. Sarcoidosis with optic nerve and retinal involvement. Arch Ophthalmol. 1976;94:945–50.

45. Biswas JMS, AtiyaAyisha BS, Agrawal A. Ocular sarcoidosis an update. KSOS. 2010;XXII:120–30.

46. Baltmr A, Lightman S, Tomkins-Netzer O. Examining the choroid in ocular inflammation: a focus on enhanced depth imaging. J Ophthalmol. 2014;2014:459136.

47. Invernizzi A, Mapelli C, Viola F, et al. Choroidal granulomas visualized by enhanced depth imaging optical coherence tomography. Retina. 2015;35:525–31.

48. Mehta H, Sim DA, Keane PA, et al. Structural changes of the choroid in sarcoid- and tuberculosis-related granulomatous uveitis. Eye (Lond). 2015;29(8):1060–8.

49. Shields CL, Kaliki S, Rojanaporn D, et al. Enhanced depth imaging optical coherence tomography of small choroidal melanoma: comparison with choroidal nevus. Arch Ophthalmol. 2012;130:850–6.

50. Hickman SJ, Quhill F, Pepper IM. The evolution of an optic nerve head granuloma due to sarcoidosis. Neuro Ophthalmol. 2016;40:59–68.

51. Pichi F, Ciardella AP. Imaging in the diagnosis and management of idiopathic retinal vasculitis, aneurysms, and neuroretinitis (IRVAN). Int Ophthalmol Clin. 2012;52:275–82.

52. Chang TS, Aylward GW, Davis JL, Mieler WF, Oliver GL, Maberley AL, et al. Idiopathic retinal vasculitis, aneurysms, and neuro-retinitis: retinal vasculitis study. Ophthalmology. 1995;102:1089–97.

53. Rao NA, Hidayat AA. Endogenous mycotic endophthalmitis: variations in clinical and histopathologic changes in candidiasis compared with aspergillosis. Am J Ophthalmol. 2001;2001(132):244–51.

54. Invernizzi A, Symes R, Miserocchi E, et al. Spectral domain optical coherence tomography findings in endogenous candida endophthalmitis and their clinical relevance. Retina. 2017;38:1011–8.

55. Roberts PK, Nesper PL, Onishi AC, et al. Characterizing photoreceptor changes in acute posterior multifocal placoid pigment epitheliopathy using adaptive optics. Retina. 2018;38:39–48.

56. Goldenberg D, Habot-Wilner Z, Loewenstein A, et al. Spectral domain optical coherence tomography classification of acute posterior multifocal placoid pigment epitheliopathy. Retina. 2012;32:1403–10.

57. Pichi F, Ciardella AP, Cunningham ET Jr, Morara M, Veronese C, Jumper JM, et al. Spectral domain optical coherence tomography findings in patients with acute syphilitic posterior placoid chorioretinopathy. Retina. 2014;34:373–84.

58. Kurup SP, Khan S, Gill MK. Spectral domain optical coherence tomography in the evaluation and management of infectious retinitis. Retina. 2014;34:2233–41.

59. Zhang M, Xin H, Roon P, et al. Infection of retinal neurons during murine cytomegalovirus retinitis. Investig Ophthalmol Vis Sci. 2005;46:2047–55.

60. Invernizzi A, Agarwal A, Ravera V, et al. Optical coherence tomography findings in cytomegalovirus retinitis: a longitudinal study. Retina. 2017;38:108–17.

61. Hugkulstone CE, Watt LL. Branch retinal arteriolar occlusion with chicken-pox. Br J Ophthalmol. 1988;72:78–80.